

ITERATIVE ALPHA EXPANSION FOR ESTIMATING GRADIENT-SPARSE SIGNALS FROM LINEAR MEASUREMENTS

SHENG XU AND ZHOU FAN

ABSTRACT. We consider estimating a piecewise-constant image, or a gradient-sparse signal on a general graph, from noisy linear measurements. We propose and study an iterative algorithm to minimize a penalized least-squares objective, with a penalty given by the “ ℓ_0 -norm” of the signal’s discrete graph gradient. The method proceeds by approximate proximal descent, applying the alpha-expansion procedure to minimize a proximal gradient in each iteration, and using a geometric decay of the penalty parameter across iterations. Under a cut-restricted isometry property for the measurement design, we prove global recovery guarantees for the estimated signal. For standard Gaussian designs, the required number of measurements is independent of the graph structure, and improves upon worst-case guarantees for total-variation (TV) compressed sensing on the 1-D and 2-D lattice graphs by polynomial and logarithmic factors, respectively. The method empirically yields lower mean-squared recovery error compared with TV regularization in regimes of moderate undersampling and moderate to high signal-to-noise, for several examples of changepoint signals and gradient-sparse phantom images.

1. INTRODUCTION

Consider an unknown signal $\mathbf{x}_* \in \mathbb{R}^p$ observed via n noisy linear measurements

$$\mathbf{y} = \mathbf{A}\mathbf{x}_* + \mathbf{e} \in \mathbb{R}^n.$$

We study the problem of estimating \mathbf{x}_* , under the assumption that its coordinates correspond to the p vertices of a given graph $G = (V, E)$, and \mathbf{x}_* is gradient-sparse. By this, we mean that

$$\|\nabla \mathbf{x}_*\|_0 \equiv \sum_{(i,j) \in E} \mathbf{1}\{x_{*,i} \neq x_{*,j}\} \quad (1)$$

is much smaller than the total number of edges $|E|$. Special cases of interest include the 1-D line graph, where variables have a sequential order and \mathbf{x}_* has a changepoint structure, and the 2-D lattice graph, where coordinates of \mathbf{x}_* represent pixels of a piecewise-constant image.

This problem has been studied since early pioneering works in compressed sensing [CRT06a, CRT06b, Don06]. Among widely-used approaches for estimating \mathbf{x}_* are those based on constraining or penalizing the total-variation (TV) semi-norm [ROF92], which may be defined (anisotropically) for a general graph as

$$\|\nabla \mathbf{x}\|_1 \equiv \sum_{(i,j) \in E} |x_i - x_j|.$$

These are examples of ℓ_1 -analysis methods [EMR07, CENR11, NDEG13], which regularize the ℓ_1 -norm of a general linear transform of \mathbf{x} rather than of its coefficients in an orthonormal basis. Related fused-lasso methods have been studied for different applications of regression and prediction in [TSR⁺05, Rin09, Tib11], other graph-based regularization methods for linear regression in [LMRW18, KG19], and trend-filtering methods regularizing higher-order discrete derivatives of \mathbf{x} in [KKBG09, WSST16].

DEPARTMENT OF STATISTICS AND DATA SCIENCE, YALE UNIVERSITY, NEW HAVEN, CT 06511
E-mail addresses: sheng.xu@yale.edu, zhou.fan@yale.edu.

Theoretical recovery guarantees for TV-regularization depend on the structure of the graph [NW13b, NW13a, CX15], and more generally on sparse conditioning properties of the pseudo-inverse ∇^\dagger for ℓ_1 -analysis methods with sparsifying transform ∇ . For direct measurements $\mathbf{A} = \mathbf{I}$, these and related issues were studied in [HR16, DHL17, FG18], which showed in particular that TV-regularization may not achieve the same worst-case recovery guarantees as analogous ℓ_0 -regularization methods on certain graphs including the 1-D line. In this setting of $\mathbf{A} = \mathbf{I}$, different computational approaches exist which may be used for approximately minimizing an ℓ_0 -regularized objective on general graphs [BVZ99, KT02, XLXJ11].

Motivated by this line of work, we propose and study an alternative to TV-regularization for the problem with indirect linear measurements $\mathbf{A} \neq \mathbf{I}$. Our procedure is based similarly on the idea of minimizing a possibly non-convex objective

$$F(\mathbf{x}) = \frac{1}{2} \|\mathbf{y} - \mathbf{A}\mathbf{x}\|_2^2 + \lambda \sum_{(i,j) \in E} c(x_i, x_j) \quad (2)$$

for an edge-associated cost function c . We will focus attention in this work on the specific choice of an ℓ_0 -regularizer

$$c(x_i, x_j) = \mathbf{1}\{x_i \neq x_j\}, \quad (3)$$

which matches (1), although the algorithm may be applied with more general choices of metric edge cost. For the above ℓ_0 edge cost, the resulting objective takes the form

$$F(\mathbf{x}) = \frac{1}{2} \|\mathbf{y} - \mathbf{A}\mathbf{x}\|_2^2 + \lambda \|\nabla \mathbf{x}\|_0.$$

We propose to minimize $F(\mathbf{x})$ using an iterative algorithm akin to proximal gradient descent: For parameters $\gamma \in (0, 1)$ and $\eta > 0$, the iterate \mathbf{x}_{k+1} is computed from \mathbf{x}_k via

$$\begin{aligned} \mathbf{a}_{k+1} &\leftarrow \mathbf{x}_k - \eta \mathbf{A}^\top (\mathbf{A}\mathbf{x}_k - \mathbf{y}) \\ \mathbf{x}_{k+1} &\leftarrow \arg \min_{\mathbf{x}} \frac{1}{2} \|\mathbf{x} - \mathbf{a}_{k+1}\|_2^2 + \lambda_k \sum_{(i,j) \in E} c(x_i, x_j) \\ \lambda_{k+1} &\leftarrow \lambda_k \cdot \gamma \end{aligned}$$

For general graphs, the second update step for \mathbf{x}_{k+1} is only approximately computable in polynomial time. We apply the alpha-expansion procedure of Boykov, Veksler, and Zabih [BVZ99] for this task, first discretizing the continuous signal domain, as analyzed statistically in [FG18]. In contrast to analogous proximal methods in convex settings [BT09, PB14], where typically $\lambda_k \equiv \lambda\eta$ is fixed across iterations, we decay λ_k geometrically from a large initial value to ensure algorithm convergence. We call the resulting algorithm ITERative ALpha Expansion, or ITALE.

Despite $F(\mathbf{x})$ being non-convex and non-smooth, we provide global recovery guarantees for a suitably chosen ITALE iterate \mathbf{x}_k . For example, under exact gradient-sparsity $\|\nabla \mathbf{x}_*\|_0 = s_*$, if \mathbf{A} consists of

$$n \gtrsim s_* \log(1 + |E|/s_*) \quad (4)$$

linear measurements with i.i.d. $\mathcal{N}(0, 1/n)$ entries, then the ITALE iterate \mathbf{x}_k for the ℓ_0 -regularizer (3) and a penalty value $\lambda_k \asymp \|\mathbf{e}\|_2^2/s_*$ satisfies with high probability

$$\|\mathbf{x}_k - \mathbf{x}_*\|_2 \lesssim \|\mathbf{e}\|_2. \quad (5)$$

More generally, we provide recovery guarantees when \mathbf{A} satisfies a certain cut-restricted isometry property, described in Definition 3.1 below. (In accordance with the compressed sensing literature, we state all theoretical guarantees for deterministic and possibly adversarial measurement error \mathbf{e} .)

Even for i.i.d. Gaussian design, we are not aware of previous polynomial-time algorithms which provably achieve this guarantees for either the 1-D line or the 2-D lattice. In particular, connecting with the above discussion, similar existing results for TV-regularization in noisy or noiseless settings require $n \gtrsim s_*(\log |E|)^3$ Gaussian measurements for the 2-D lattice and $n \gtrsim \sqrt{|E|s_*} \log |E|$

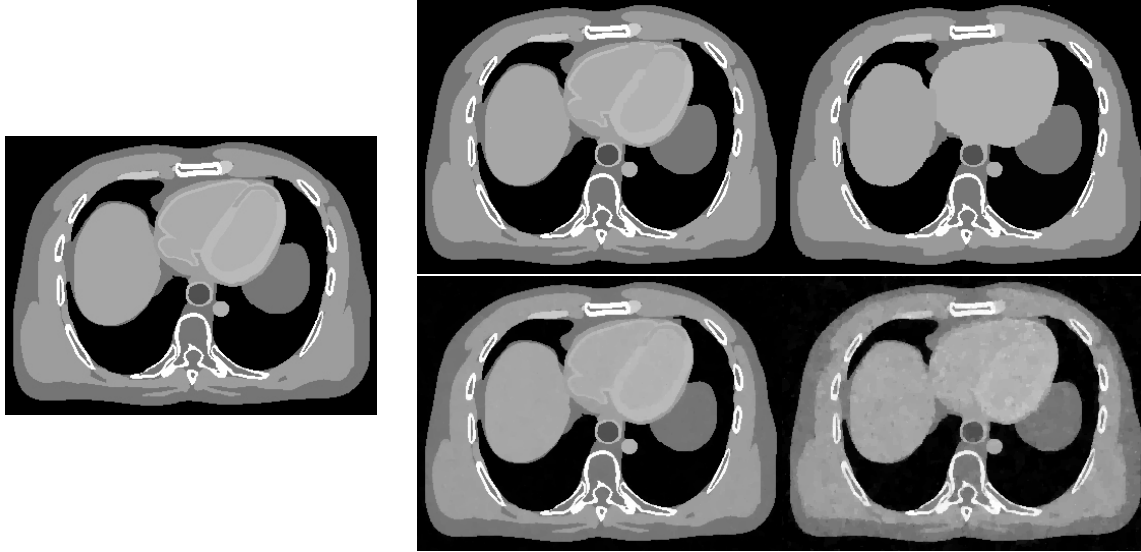


FIGURE 1. Left: Original image slice from the XCAT digital phantom. Top row: $\hat{\mathbf{x}}^{\text{ITALE}}$ from 20% undersampled and reweighted Fourier measurements, in low noise ($\sigma = 4$, left) and medium noise ($\sigma = 16$, right) settings. Bottom row: $\hat{\mathbf{x}}^{\text{TV}}$ for the same measurements.

measurements for the 1-D line [NW13b, CX15]. In contrast, for lattice graphs of dimensions 3 and higher where the Laplacian $\mathbf{L} = \nabla^T \nabla$ is well-conditioned, as well as for more general ℓ_1 -analysis methods where ∇^\dagger is a tight frame, optimal recovery guarantees for TV/ ℓ_1 -regularization hold with $n \gtrsim s_* \log |E|$ or $n \gtrsim s_* \log(|E|/s_*)$ measurements as expected [CENR11, NW13a, CX15]. ITALE provides this guarantee up to a constant factor, irrespective of the graph structure.

In practice, for γ sufficiently close to 1, we directly interpret the sequence of ITALE iterates \mathbf{x}_k as approximate minimizers of the objective function (2) for penalty parameters $\lambda = \lambda_k/\eta$ along a regularization path. We select the iterate k using cross-validation on the prediction error for \mathbf{y} , and we use the final estimate $\hat{\mathbf{x}}^{\text{ITALE}} = \mathbf{x}_k$. Figure 1 compares in simulation $\hat{\mathbf{x}}^{\text{ITALE}}$ using the ℓ_0 -regularizer (3) with $\hat{\mathbf{x}}^{\text{TV}}$ (globally) minimizing the TV-regularized objective

$$F^{\text{TV}}(\mathbf{x}) = \frac{1}{2} \|\mathbf{y} - \mathbf{A}\mathbf{x}\|_2^2 + \lambda \|\nabla \mathbf{x}\|_1, \quad (6)$$

with λ selected also using cross-validation. The example depicts a synthetic image of a human chest slice, previously generated by [GHG⁺17] using the XCAT digital phantom [SSM⁺10]. The design \mathbf{A} is an undersampled and reweighted Fourier matrix, using a sampling scheme described in Section 3 and similar to that proposed in [KW14] for TV-regularized compressed sensing. In a low-noise setting, a detailed comparison of the recovered images reveals that $\hat{\mathbf{x}}^{\text{ITALE}}$ provides a sharper reconstruction than $\hat{\mathbf{x}}^{\text{TV}}$. As noise increases, $\hat{\mathbf{x}}^{\text{TV}}$ becomes blotchy, while $\hat{\mathbf{x}}^{\text{ITALE}}$ begins to lose finer image details. Quantitative comparisons of recovery error are provided in Section 4.2 and are favorable towards ITALE in lower noise regimes.

ITALE is similar to some methods oriented towards ℓ_0 -regularized sparse regression and signal recovery [TG07, Zha11, BKM16], including notably the Iterative Hard Thresholding (IHT) [BD09] and CoSaMP [NT09] methods in compressed sensing. We highlight here several differences:

- For sparsity in an orthonormal basis, forward stepwise selection and orthogonal matching pursuit provide greedy “ ℓ_0 ” approaches to variable selection, also with provable guarantees [TG07, Zha11, EKDN18]. However, such methods do not have direct analogues for gradient-sparsity in graphs, as one cannot select a single edge difference $x_i - x_j$ to be nonzero without changing other edge differences.

- IHT and CoSaMP enforce sparsity of \mathbf{x}_{k+1} in each iteration by projecting to the s largest coordinates of \mathbf{a}_{k+1} , for user-specified s . In contrast, ITALE uses a Lagrangian form that penalizes (rather than constrains) $\|\nabla \mathbf{x}_{k+1}\|_0$. This is partly for computational reasons, as we are not aware of fast algorithms that can directly perform such a projection step onto the (non-convex) set $\{\mathbf{x} : \|\nabla \mathbf{x}\|_0 \leq s\}$ for general graphs. Our theoretical convergence analysis handles this Lagrangian form.
- In contrast to more general-purpose mixed-integer optimization procedures in [BKM16], each iterate of ITALE (and hence also the full algorithm, for a polynomial number of iterations) is provably polynomial-time in the input size $(n, p, |E|)$ [FG18]. On our personal computer, for the $p = 360 \times 270 = 97200$ image of Figure 1, computing the 60 iterates constituting a full ITALE solution path required about 20 minutes, using the optimized alpha-expansion code of [BK04].

While our theoretical focus is on ℓ_0 -regularization, we expect that for certain regimes of under-sampling and signal-to-noise, improved empirical recovery may be possible with edge costs $c(x_i, x_j)$ interpolating between the ℓ_0 and ℓ_1 penalties. These are applicable in the ITALE algorithm and would be interesting to investigate in future work.

2. MODEL AND ALGORITHM

Let $G = (V, E)$ be a given connected graph on the vertices $V = \{1, \dots, p\}$, with undirected edge set E . We assume throughout that $p \geq 3$. For a signal vector $\mathbf{x}_* \in \mathbb{R}^p$, measurement matrix $\mathbf{A} \in \mathbb{R}^{n \times p}$, and measurement errors $\mathbf{e} \in \mathbb{R}^n$, we observe

$$\mathbf{y} = \mathbf{A}\mathbf{x}_* + \mathbf{e} \in \mathbb{R}^n. \quad (7)$$

Denote by $\nabla \in \{-1, 0, 1\}^{|E| \times p}$ the discrete gradient matrix on the graph G , defined¹ by

$$\nabla \mathbf{x} = (x_i - x_j : (i, j) \in E) \in \mathbb{R}^{|E|}.$$

We study estimation of \mathbf{x}_* , assuming that \mathbf{x}_* has (or is well-approximated by a signal having) small exact gradient sparsity $\|\nabla \mathbf{x}_*\|_0$.

Our proposed algorithm is an iterative approach called ITALE, presented as Algorithm 1. It is based around the idea of minimizing the objective (2). In this objective, the cost function $c : \mathbb{R}^2 \rightarrow \mathbb{R}$ must satisfy the metric properties

$$c(x, y) = c(y, x) \geq 0, \quad c(x, x) = 0 \Leftrightarrow x = 0, \quad c(x, z) \leq c(x, y) + c(y, z), \quad (8)$$

but is otherwise general. Importantly, c may be non-smooth and non-convex. The algorithm applies proximal descent, alternating between constructing a surrogate signal \mathbf{a}_{k+1} in line 3 and denoising this surrogate signal in line 4, discussed in more detail below.

Some intuition for \mathbf{a}_{k+1} is provided by considering the setting $\mathbf{e} \approx \mathbf{0}$ and $\eta \mathbf{A}^\top \mathbf{A} \approx \mathbf{I}$, in which case

$$\begin{aligned} \mathbf{a}_{k+1} &= \mathbf{x}_k - \eta \mathbf{A}^\top (\mathbf{A} \mathbf{x}_k - \mathbf{y}) \\ &= \mathbf{x}_* + (\mathbf{I} - \eta \mathbf{A}^\top \mathbf{A})(\mathbf{x}_k - \mathbf{x}_*) + \eta \mathbf{A}^\top \mathbf{e} \approx \mathbf{x}_*. \end{aligned}$$

There are two sources of noise $(\mathbf{I} - \eta \mathbf{A}^\top \mathbf{A})(\mathbf{x}_k - \mathbf{x}_*)$ and $\eta \mathbf{A}^\top \mathbf{e}$ in \mathbf{a}_{k+1} , the former expected to decrease across iterations as the reconstruction error $\|\mathbf{x}_k - \mathbf{x}_*\|$ decreases. A tuning parameter λ_k is applied to denoise \mathbf{a}_{k+1} in each iteration, where λ_k also decreases across iterations to match the noise level. Our theoretical analysis indicates to use a geometric rate of decay $\lambda_{k+1} = \lambda_k \cdot \gamma$, starting from a large initial value λ_{\max} .

ITALE yields iterates $\mathbf{x}_1, \mathbf{x}_2, \dots, \mathbf{x}_K$, which we directly interpret as recovered signals along a regularization path for different choices of $\lambda \equiv \lambda_k / \eta$ in the objective (2). We choose λ_{\max} such that

¹Here, we may fix an arbitrary ordering of the vertex pair (i, j) for each edge.

Algorithm 1 Iterative Alpha Expansion

Input: $\mathbf{y} \in \mathbb{R}^n$, $\mathbf{A} \in \mathbb{R}^{n \times p}$, and parameters $\gamma \in (0, 1)$, $\lambda_{\max} > \lambda_{\min} > 0$, and $\eta, \delta > 0$.

- 1: Initialize $\mathbf{x}_0 \leftarrow \mathbf{0}$, $\lambda_0 \leftarrow \lambda_{\max}$
- 2: **for** $k = 0, 1, 2, \dots, K$ until $\lambda_K < \lambda_{\min}$ **do**
- 3: $\mathbf{a}_{k+1} \leftarrow \mathbf{x}_k - \eta \mathbf{A}^\top (\mathbf{A} \mathbf{x}_k - \mathbf{y})$
- 4: $\mathbf{x}_{k+1} \leftarrow \text{AlphaExpansion}(\mathbf{a}_{k+1}, \lambda_k, \delta)$
- 5: $\lambda_{k+1} \leftarrow \lambda_k \cdot \gamma$
- 6: **end for**

Output: $\mathbf{x}_1, \dots, \mathbf{x}_K$

the initial iterates oversmooth \mathbf{x}_* , and λ_{\min} such that the final iterates undersmooth \mathbf{x}_* . We remark that an alternative approach would be to iterate lines 3 and 4 in Algorithm 1 until convergence for each λ_k , before updating λ_k to the next value λ_{k+1} . However, we find that this is not necessary in practice if γ is chosen close enough to 1, and our stated algorithm achieves a computational speed-up compared to this approach.

To perform the denoising in line 4, ITALE applies the alpha-expansion graph cut procedure from [BVZ99] to approximately solve the minimization problem

$$\min_{\mathbf{x} \in \mathbb{R}^p} \frac{1}{2} \|\mathbf{x} - \mathbf{a}_{k+1}\|_2^2 + \lambda_k \sum_{(i,j) \in E} c(x_i, x_j).$$

This sub-routine is denoted as $\text{AlphaExpansion}(\mathbf{a}_{k+1}, \lambda_k, \delta)$, and is described in Algorithm 2 for completeness. At a high level, the alpha-expansion method encodes the above objective function in the structure of an edge-weighted augmented graph, and iterates over global moves that swap the signal value on a subset of vertices for a given new value by finding a minimum graph cut. The original alpha-expansion algorithm of [BVZ99] computes an approximate maximum-a-posteriori estimate in a discrete Potts model with a metric edge-cost satisfying (8). To apply this to a continuous signal domain, we restrict coordinate values of \mathbf{x} to a discrete grid

$$\delta\mathbb{Z} = \{k\delta : k \in \mathbb{Z}\}.$$

Here, δ is a small user-specified discretization parameter. As shown in [FG18, Lemma S2.1] (see also [BVZ99, Theorem 6.1]), the output $\mathbf{x}_{k+1} = \text{AlphaExpansion}(\mathbf{a}_{k+1}, \lambda_k, \delta)$ has the deterministic guarantee

$$\frac{1}{2} \|\mathbf{x}_{k+1} - \mathbf{a}_{k+1}\|_2^2 + \lambda_k \sum_{(i,j) \in E} c(x_i, x_j) \leq \min_{\mathbf{x} \in (\delta\mathbb{Z})^p} \left(\frac{1}{2} \|\mathbf{x} - \mathbf{a}_{k+1}\|_2^2 + 2\lambda_k \sum_{(i,j) \in E} c(x_i, x_j) \right) \quad (9)$$

with the additional factor of 2 applying to the penalty on the right side. This guarantee is important for the theoretical recovery properties that we will establish in Section 3.

We make a few remarks regarding parameter tuning in practice:

- Using conservative choices for λ_{\max} (large), γ (close to 1), and δ (small) increases the total runtime of the procedure, but does not degrade the quality of recovery. In our experiments, we fix $\gamma = 0.9$ and set δ in each iteration to yield 300 grid values for $\delta\mathbb{Z} \cap [a_{\min}, a_{\max}]$ in Algorithm 2.
- We monitor the gradient sparsity $\|\nabla \mathbf{x}_k\|_0$ across iterations, and terminate the algorithm when $\|\nabla \mathbf{x}_K\|_0$ exceeds a certain fraction (e.g. 50%) of the total number of edges $|E|$, rather than fixing λ_{\min} .
- The parameter η should be matched to the scaling and restricted isometry properties of the design matrix \mathbf{A} . For sub-Gaussian and Fourier designs scaled by $1/\sqrt{n}$ as in Propositions 3.2 and 3.3 below, we set $\eta = 1$.

Algorithm 2 AlphaExpansion($\mathbf{a}, \lambda, \delta$) subroutine

Input: $\mathbf{a} \in \mathbb{R}^p$, cost function $c : \mathbb{R}^2 \rightarrow \mathbb{R}$, parameters $\lambda, \delta > 0$.

- 1: Let a_{\min}, a_{\max} be the minimum and maximum values of \mathbf{a} . Initialize $\mathbf{x} \in \mathbb{R}^p$ arbitrarily.
- 2: **loop**
- 3: **for** each $z \in \delta\mathbb{Z} \cap [a_{\min}, a_{\max}]$ **do**
- 4: Construct the following edge-weighted augmentation $G_{z,\mathbf{x}}$ of the graph G :
- 5: Introduce a source vertex s and a sink vertex t , connect s to each $i \in \{1, \dots, p\}$ with weight $\frac{1}{2}(a_i - z)^2$, and connect t to each $i \in \{1, \dots, p\}$ with weight $\frac{1}{2}(a_i - x_i)^2$ if $x_i \neq z$, or weight ∞ if $x_i = z$.
- 6: **for** each edge $\{i, j\} \in E$ **do**
- 7: **if** $x_i = x_j$ **then**
- 8: Assign weight $\lambda c(x_i, z)$ to $\{i, j\}$.
- 9: **else**
- 10: Introduce a new vertex $v_{i,j}$, and replace edge $\{i, j\}$ by the three edges $\{i, v_{i,j}\}$, $\{j, v_{i,j}\}$, and $\{t, v_{i,j}\}$, with weights $\lambda c(x_i, z)$, $\lambda c(x_j, z)$, and $\lambda c(x_i, x_j)$ respectively.
- 11: **end if**
- 12: **end for**
- 13: Find the minimum s-t cut (S, T) of $G_{z,\mathbf{x}}$ such that $s \in S$ and $t \in T$.
- 14: For each $i \in \{1, \dots, p\}$, update $x_i \leftarrow z$ if $i \in T$, and keep x_i unchanged if $i \in S$.
- 15: **end for**
- 16: If \mathbf{x} was unchanged for each z above, then return \mathbf{x} .
- 17: **end loop**

Output: \mathbf{x}

- The most important tuning parameter is the iterate k for which we take the final estimate $\hat{\mathbf{x}}^{\text{ITALE}} = \mathbf{x}_k$. In practice, we apply cross-validation on the mean-squared prediction error for \mathbf{y} to select k . Note that η should be rescaled by the number of training samples in each fold, i.e. for 5-fold cross-validation with training sample size $0.8n$, we set $\eta = 1/0.8$ instead of $\eta = 1$ in the cross-validation runs.

3. RECOVERY GUARANTEES

We provide in this section theoretical guarantees on the recovery error $\|\hat{\mathbf{x}}^{\text{ITALE}} - \mathbf{x}_*\|_2$, where $\hat{\mathbf{x}}^{\text{ITALE}} \equiv \mathbf{x}_k$ for a deterministic (non-adaptive) choice of iterate k . Throughout this section, ITALE is assumed to be applied with the ℓ_0 edge cost $c(x_i, x_j) = \mathbf{1}\{x_i \neq x_j\}$.

3.1. cRIP condition. Our primary assumption on the measurement design \mathbf{A} will be the following version of a restricted isometry property.

Definition 3.1. Let $\kappa > 0$, and let $\rho : [0, \infty) \rightarrow [0, \infty)$ be any function satisfying $\rho'(s) \geq 0$ and $\rho''(s) \leq 0$ for all $s > 0$. A matrix $\mathbf{A} \in \mathbb{R}^{n \times p}$ satisfies the (κ, ρ) -**cut-restricted isometry property** (cRIP) if, for every $\mathbf{x} \in \mathbb{R}^p$ with $\|\nabla \mathbf{x}\|_0 \geq 1$, we have

$$\left(1 - \kappa - \sqrt{\rho(\|\nabla \mathbf{x}\|_0)}\right) \|\mathbf{x}\|_2 \leq \|\mathbf{A}\mathbf{x}\|_2 \leq \left(1 + \kappa + \sqrt{\rho(\|\nabla \mathbf{x}\|_0)}\right) \|\mathbf{x}\|_2.$$

This definition depends implicitly on the structure of the underlying graph G , via its discrete gradient matrix ∇ . Examples of the function ρ are given in the two propositions below.

This condition is stronger than the usual RIP condition in compressed sensing [CRT06a, CRT06b] in two ways: First, Definition 3.1 requires quantitative control of $\|\mathbf{A}\mathbf{x}\|_2$ for *all* vectors $\mathbf{x} \in \mathbb{R}^p$, rather than only those with sparsity $\|\nabla \mathbf{x}\|_0 \leq s$ for some specified s . We use this in our analysis to handle regularization of $\|\nabla \mathbf{x}\|_0$ in Lagrangian (rather than constrained) form. Second, approximate

isometry is required for signals with small gradient-sparsity $\|\nabla \mathbf{x}\|_0$, rather than small sparsity $\|\mathbf{x}\|_0$. For graphs with bounded maximum degree, all sparse signals are also gradient-sparse, so this is indeed stronger up to a relabeling of constants. This requirement is similar to the D-RIP condition of [CENR11] for general sparse analysis models, and is also related to the condition of [NW13b] that $\mathbf{A}\mathcal{H}^{-1}$ satisfies the usual RIP condition, where \mathcal{H}^{-1} is the inverse Haar-wavelet transform on the 2-D lattice.

Despite this strengthening of the required RIP condition, Definition 3.1 still holds for sub-Gaussian designs \mathbf{A} , where κ depends on the condition number of the design covariance. We defer the proof of the following result to Appendix B. For a random vector \mathbf{a} , we denote its sub-Gaussian norm as

$$\|\mathbf{a}\|_{\psi_2} = \sup_{\mathbf{u}: \|\mathbf{u}\|_2=1} \sup_{k \geq 1} k^{-1/2} \mathbb{E} \left[|\mathbf{u}^\top \mathbf{a}|^k \right]^{1/k},$$

and say that \mathbf{a} is sub-Gaussian if $\|\mathbf{a}\|_{\psi_2} \leq K$ for a constant $K > 0$.

Proposition 3.2. *Let $\mathbf{A} \in \mathbb{R}^{n \times p}$ have i.i.d. rows \mathbf{a}_i/\sqrt{n} , where $\text{Cov}[\mathbf{a}_i] = \boldsymbol{\Sigma}$ and $\|\mathbf{a}_i\|_{\psi_2} \leq K$. Suppose that the largest and smallest eigenvalues of $\boldsymbol{\Sigma}$ satisfy $\sigma_{\max}(\boldsymbol{\Sigma}) \leq (1 + \kappa)^2$ and $\sigma_{\min}(\boldsymbol{\Sigma}) \geq (1 - \kappa)^2$ for a constant $\kappa \in (0, 1)$. Then for any $k > 0$ and some constant $C > 0$ depending only on K, κ, k , with probability at least $1 - |E|^{-k}$, the matrix \mathbf{A} satisfies (κ, ρ) -cRIP for the function*

$$\rho(s) = \frac{Cs \log(1 + |E|/s)}{n}.$$

For large 2-D images, using Fourier measurements with matrix multiplication implemented by an FFT can significantly reduce the runtime of Algorithm 1. As previously discussed in [LDP07, NW13b, KW14], uniform random sampling of Fourier coefficients may not be appropriate for reconstructing piecewise-constant images, as these typically have larger coefficients in the lower Fourier frequencies. We instead study a non-uniform sampling and reweighting scheme similar to that proposed in [KW14] for total-variation compressed sensing, and show that Definition 3.1 also holds for this reweighted Fourier matrix.

For $p = N_1 N_2$ and N_1, N_2 both powers of 2, let $\mathcal{F} \in \mathbb{C}^{p \times p}$ be the 2-D discrete Fourier matrix on the lattice graph G of size $N_1 \times N_2$, normalized such that $\mathcal{F}\mathcal{F}^* = \mathbf{I}$. We define this as the Kronecker product $\mathcal{F} = \mathcal{F}^1 \otimes \mathcal{F}^2$, where $\mathcal{F}^1 \in \mathbb{C}^{N_1 \times N_1}$ is the 1-D discrete Fourier matrix with entries

$$\mathcal{F}_{jk}^1 = \frac{1}{\sqrt{N_1}} \cdot e^{2\pi i \frac{(j-1)(k-1)}{N_1}},$$

and $\mathcal{F}^2 \in \mathbb{C}^{N_2 \times N_2}$ is defined analogously. (Thus rows closer to $N_1/2 + 1$ in \mathcal{F}^1 correspond to higher frequency components.) Let $\mathcal{F}_{(i,j)}^*$ denote row (i, j) of \mathcal{F} , where we index by pairs $(i, j) \in \{1, \dots, N_1\} \times \{1, \dots, N_2\}$ corresponding to the Kronecker structure. We define a sampled Fourier matrix as follows: Let ν_1 be the probability mass function on $\{1, \dots, N_1\}$ given by

$$\nu_1(i) \propto \frac{1}{C_0 + \min(i-1, N_1 - i + 1)}, \quad C_0 \geq 1. \quad (10)$$

Define similarly ν_2 on $\{1, \dots, N_2\}$, and let $\nu = \nu_1 \times \nu_2$. For a given number of measurements n , draw $(i_1, j_1), \dots, (i_n, j_n) \stackrel{iid}{\sim} \nu$, and set

$$\tilde{\mathbf{A}} = \frac{1}{\sqrt{n}} \begin{pmatrix} \mathcal{F}_{(i_1, j_1)}^* / \sqrt{\nu(i_1, j_1)} \\ \vdots \\ \mathcal{F}_{(i_n, j_n)}^* / \sqrt{\nu(i_n, j_n)} \end{pmatrix} \in \mathbb{C}^{n \times p}. \quad (11)$$

Proposition 3.3. *Let G be the 2-D lattice graph of size $N_1 \times N_2$, where N_1, N_2 are powers of 2 and $1/K < N_1/N_2 < K$ for a constant $K > 0$. Set $p = N_1 N_2$ and let $\tilde{\mathbf{A}}$ be the matrix defined in*

(11). Then for some constants $C, t_0 > 0$ depending only on K , and for any $t > t_0$, with probability at least $1 - e^{-(\log n)(\log p)^3} - p^{-t}$, $\tilde{\mathbf{A}}$ satisfies the (κ, ρ) -cRIP with $\kappa = 0$ and

$$\rho(s) = Cts \frac{(\log p)^8 \log n}{n}.$$

We defer the proof also to Appendix B. This proposition pertains to the complex analogue of Definition 3.1, where $\tilde{\mathbf{A}}, \mathbf{x}$ are allowed to be complex-valued, and $\|\cdot\|_2$ denotes the complex ℓ_2 -norm. For a real-valued signal $\mathbf{x}_* \in \mathbb{R}^p$, Algorithm 1 may be applied to $\tilde{\mathbf{y}} = \tilde{\mathbf{A}}\mathbf{x}_* + \mathbf{e} \in \mathbb{C}^n$ by separating real and imaginary parts of $\tilde{\mathbf{y}}$ into a real vector $\mathbf{y} \in \mathbb{R}^{2n}$. The corresponding $\mathbf{A} \in \mathbb{R}^{2n \times p}$ satisfies $\|\mathbf{A}\mathbf{x}\|_2 = \|\tilde{\mathbf{A}}\mathbf{x}\|_2$, so the same cRIP condition holds (in the real sense) for \mathbf{A} .

3.2. Recovery error bounds. To illustrate the idea of analysis, we first establish a result showing that ITALE can yield exact recovery in a setting of no measurement noise. We require \mathbf{x}_* to be gradient-sparse with coordinates belonging exactly to $\delta\mathbb{Z}$, as the ITALE output has this latter property. Discretization error will be addressed in our subsequent result.

Theorem 3.4. *Suppose $\mathbf{e} = \mathbf{0}$ and $\mathbf{x}_* \in (\delta\mathbb{Z})^p$, and denote $s_* = \max(\|\nabla\mathbf{x}_*\|_0, 1)$. Suppose $\sqrt{\eta} \cdot \mathbf{A}$ satisfies (κ, ρ) -cRIP, where $\kappa \in [0, \sqrt{3/2} - 1)$. Set $t(\kappa) = 1 - 4\kappa - 2\kappa^2 \in (0, 1]$, and choose tuning parameters*

$$\left(1 - \frac{t(\kappa)}{4}\right)^2 < \gamma < 1, \quad \lambda_{\max} > \|\mathbf{x}_*\|_2^2.$$

For some constants $C, c > 0$ depending only on κ , if

$$\rho(s_*) \leq c,$$

then each iterate \mathbf{x}_k of Algorithm 1 satisfies

$$\|\mathbf{x}_k - \mathbf{x}_*\|_2 \leq C\sqrt{\lambda_{\max}s_*} \cdot \gamma^{k/2}. \quad (12)$$

In particular, $\mathbf{x}_k = \mathbf{x}_*$ for all sufficiently large k .

Thus, in this noiseless setting, the iterates exhibit linear convergence to the true signal \mathbf{x}_* . The required condition $\rho(s_*) \leq c$ translates into a requirement of

$$n \gtrsim s_* \log(1 + |E|/s_*)$$

measurements for \mathbf{A} having i.i.d. $\mathcal{N}(0, 1/n)$ entries, by Proposition 3.2, or

$$n \gtrsim s_*(\log p)^8 \log \log p$$

weighted Fourier measurements for the 2-D lattice graph, as defined in Proposition 3.3. For these designs, (κ, ρ) -cRIP holds for $\sqrt{\eta} \cdot \mathbf{A}$ where $\kappa = 0$ and $\eta = 1$.

Proof of Theorem 3.4. Denote

$$s_k = \|\nabla\mathbf{x}_k\|_0, \quad \mathbf{r}_k = \mathbf{x}_k - \mathbf{x}_*.$$

Applying the optimality condition (9) to compare \mathbf{x}_{k+1} with $\mathbf{x}_* = \mathbf{x}_k - \mathbf{r}_k$, we obtain

$$\|\mathbf{x}_{k+1} - \mathbf{a}_{k+1}\|_2^2 + 2\lambda_k s_{k+1} \leq \|\mathbf{x}_k - \mathbf{r}_k - \mathbf{a}_{k+1}\|_2^2 + 4\lambda_k s_*. \quad (13)$$

Let \mathcal{S}_k be the partition of $\{1, \dots, p\}$ induced by the piecewise-constant structure of \mathbf{x}_k : Each element of \mathcal{S}_k corresponds to a connected subgraph of G on which \mathbf{x}_k takes a constant value. Let $\mathcal{S}_{k+1}, \mathcal{S}_*$ similarly be the partitions induced by $\mathbf{x}_{k+1}, \mathbf{x}_*$, and denote by \mathcal{S} the common refinement of $\mathcal{S}_k, \mathcal{S}_{k+1}, \mathcal{S}_*$. Defining the boundary

$$\partial\mathcal{S} = \{(i, j) \in E : i, j \text{ belong to different elements of } \mathcal{S}\},$$

observe that each edge $(i, j) \in \partial S$ must be such that at least one of \mathbf{x}_k , \mathbf{x}_{k+1} , or \mathbf{x}_* takes different values at its two endpoints. Then

$$|\partial S| \leq s_* + s_k + s_{k+1}. \quad (14)$$

Let $\mathbf{P} : \mathbb{R}^p \rightarrow \mathbb{R}^p$ be the orthogonal projection onto the subspace of signals taking a constant value over each element of \mathcal{S} , and let $\mathbf{P}^\perp = \mathbf{I} - \mathbf{P}$. Then $\mathbf{x}_{k+1}, \mathbf{x}_k, \mathbf{r}_k$ all belong to the range of \mathbf{P} , so an orthogonal decomposition yields

$$\begin{aligned} \|\mathbf{x}_{k+1} - \mathbf{a}_{k+1}\|_2^2 &= \|\mathbf{x}_{k+1} - \mathbf{P}\mathbf{a}_{k+1}\|_2^2 + \|\mathbf{P}^\perp \mathbf{a}_{k+1}\|_2^2, \\ \|\mathbf{x}_k - \mathbf{r}_k - \mathbf{a}_{k+1}\|_2^2 &= \|\mathbf{x}_k - \mathbf{r}_k - \mathbf{P}\mathbf{a}_{k+1}\|_2^2 + \|\mathbf{P}^\perp \mathbf{a}_{k+1}\|_2^2. \end{aligned}$$

Applying this, the definition (in the noiseless setting $\mathbf{e} = \mathbf{0}$)

$$\mathbf{a}_{k+1} = \mathbf{x}_k - \eta \mathbf{A}^\top (\mathbf{A}\mathbf{x}_k - \mathbf{y}) = \mathbf{x}_k - \eta \mathbf{A}^\top \mathbf{A}\mathbf{r}_k,$$

and the condition $\mathbf{P}\mathbf{x}_k = \mathbf{x}_k$ to (13), we obtain

$$\|\mathbf{x}_{k+1} - \mathbf{x}_k + \eta \mathbf{P}\mathbf{A}^\top \mathbf{A}\mathbf{r}_k\|_2^2 \leq \|\eta \mathbf{P}\mathbf{A}^\top \mathbf{A}\mathbf{r}_k - \mathbf{r}_k\|_2^2 + \lambda_k (4s_* - 2s_{k+1}).$$

Applying the triangle inequality and $\mathbf{x}_{k+1} - \mathbf{x}_k = \mathbf{r}_{k+1} - \mathbf{r}_k$,

$$\left(\|\mathbf{r}_{k+1}\|_2 - \|\mathbf{r}_k - \eta \mathbf{P}\mathbf{A}^\top \mathbf{A}\mathbf{r}_k\|_2 \right)_+^2 \leq \|\mathbf{r}_k - \eta \mathbf{P}\mathbf{A}^\top \mathbf{A}\mathbf{r}_k\|_2^2 + \lambda_k (4s_* - 2s_{k+1}). \quad (15)$$

We derive from this two consequences: First, lower-bounding the left side by 0 and rearranging,

$$\lambda_k s_{k+1} \leq \frac{1}{2} \|\mathbf{r}_k - \eta \mathbf{P}\mathbf{A}^\top \mathbf{A}\mathbf{r}_k\|_2^2 + 2\lambda_k s_* \leq \|\mathbf{r}_k\|_2^2 + \|\sqrt{\eta} \mathbf{A}\mathbf{P}\|_{\text{op}}^2 \cdot \|\sqrt{\eta} \mathbf{A}\mathbf{r}_k\|_2^2 + 2\lambda_k s_*. \quad (16)$$

The condition (14) and definition of \mathbf{P} imply, for any $\mathbf{u} \in \mathbb{R}^p$, that $\|\nabla(\mathbf{P}\mathbf{u})\|_0 \leq s_* + s_k + s_{k+1}$. The definition of \mathbf{r}_k implies $\|\nabla \mathbf{r}_k\|_0 \leq s_* + s_k$. Setting

$$\tau_k = \kappa + \sqrt{\rho(s_* + s_k + s_{k+1})}, \quad \zeta_k = \kappa + \sqrt{\rho(s_* + s_k)}$$

we deduce from the (κ, ρ) -cRIP condition for $\sqrt{\eta} \cdot \mathbf{A}$ that

$$\|\sqrt{\eta} \mathbf{A}\mathbf{P}\|_{\text{op}}^2 = \sup_{\mathbf{u} \in \mathbb{R}^p: \|\mathbf{u}\|_2=1} \|\sqrt{\eta} \mathbf{A}\mathbf{P}\mathbf{u}\|_2^2 \leq (1 + \tau_k)^2, \quad \|\sqrt{\eta} \mathbf{A}\mathbf{r}_k\|_2^2 \leq (1 + \zeta_k)^2 \|\mathbf{r}_k\|_2^2. \quad (17)$$

Note that since $\rho(s)$ and $\sqrt{\rho(s)}$ are both nonnegative and concave by Definition 3.1, we have

$$\rho'(s) \leq (\rho(s) - \rho(0))/s \leq \rho(s)/s, \quad \frac{d}{ds}[\sqrt{\rho(s)}] \leq (\sqrt{\rho(s)} - \sqrt{\rho(0)})/s \leq \sqrt{\rho(s)}/s.$$

The function

$$f_k(s) = \left(1 + \kappa + \sqrt{\rho(s_* + s_k + s)} \right)^2$$

is also increasing and concave, and by the above, its derivative at $s = 0$ satisfies

$$f'_k(0) \leq d_k/(s_* + s_k), \quad d_k \equiv 2(1 + \kappa)\sqrt{\rho(s_* + s_k)} + \rho(s_* + s_k).$$

Thus

$$(1 + \tau_k)^2 = f_k(s_{k+1}) \leq f_k(0) + f'_k(0) \cdot s_{k+1} \leq (1 + \zeta_k)^2 + d_k s_{k+1}/s_*. \quad (18)$$

Applying this and (17) to (16), we get

$$\begin{aligned} \lambda_k s_{k+1} &\leq \left(1 + (1 + \tau_k)^2 (1 + \zeta_k)^2 \right) \|\mathbf{r}_k\|_2^2 + 2\lambda_k s_* \\ &\leq \left(1 + (1 + \zeta_k)^4 + (1 + \zeta_k)^2 d_k s_{k+1}/s_* \right) \|\mathbf{r}_k\|_2^2 + 2\lambda_k s_*. \end{aligned}$$

Rearranging gives

$$\left(\lambda_k - (1 + \zeta_k)^2 d_k \|\mathbf{r}_k\|_2^2 / s_* \right) \cdot s_{k+1} \leq \left(1 + (1 + \zeta_k)^4 \right) \cdot \|\mathbf{r}_k\|_2^2 + 2\lambda_k s_*. \quad (19)$$

Second, applying the (κ, ρ) -cRIP condition for $\sqrt{\eta} \cdot \mathbf{A}$ again, we have for every $\mathbf{u} \in \mathbb{R}^p$

$$\begin{aligned} \left| \mathbf{u}^\top (\eta \mathbf{P} \mathbf{A}^\top \mathbf{A} \mathbf{P} - \mathbf{P}) \mathbf{u} \right| &= \left| \|\sqrt{\eta} \mathbf{A} \mathbf{P} \mathbf{u}\|_2^2 - \|\mathbf{P} \mathbf{u}\|_2^2 \right| \\ &\leq \max \left(|1 - (1 - \tau_k)^2|, |1 - (1 + \tau_k)^2| \right) \|\mathbf{P} \mathbf{u}\|_2^2 = (2\tau_k + \tau_k^2) \|\mathbf{P} \mathbf{u}\|_2^2. \end{aligned}$$

So $\|\eta \mathbf{P} \mathbf{A}^\top \mathbf{A} \mathbf{P} - \mathbf{P}\|_{\text{op}} \leq 2\tau_k + \tau_k^2$. Then, as $\mathbf{r}_k = \mathbf{P} \mathbf{r}_k$, we get from (15) that

$$\left(\|\mathbf{r}_{k+1}\|_2 - (2\tau_k + \tau_k^2) \|\mathbf{r}_k\|_2 \right)_+^2 \leq (2\tau_k + \tau_k^2)^2 \|\mathbf{r}_k\|_2^2 + \lambda_k (4s_* - 2s_{k+1}).$$

Taking the square-root and applying $\sqrt{x+y} \leq \sqrt{x} + \sqrt{y}$,

$$\|\mathbf{r}_{k+1}\|_2 \leq (4\tau_k + 2\tau_k^2) \|\mathbf{r}_k\|_2 + \sqrt{\lambda_k (4s_* - 2s_{k+1})_+}$$

Applying the definitions of τ_k and $t(\kappa)$,

$$4\tau_k + 2\tau_k^2 \leq 1 - t(\kappa) + 4(1 + \kappa) \sqrt{\rho(s_* + s_k + s_{k+1})} + 2\rho(s_* + s_k + s_{k+1}).$$

Thus

$$\|\mathbf{r}_{k+1}\|_2 \leq \left[1 - t(\kappa) + 4(1 + \kappa) \sqrt{\rho(s_* + s_k + s_{k+1})} + 2\rho(s_* + s_k + s_{k+1}) \right] \cdot \|\mathbf{r}_k\|_2 + \sqrt{4\lambda_k s_*}. \quad (20)$$

We now claim by induction on k that, if $\rho(s_*) \leq c_0$ for a sufficiently small constant $c_0 > 0$, then

$$s_k \leq \frac{90}{t(\kappa)^2} s_*, \quad \|\mathbf{r}_k\|_2 \leq \frac{4\sqrt{\lambda_k s_*}}{t(\kappa)} \quad (21)$$

for every k . For $k = 0$, these are satisfied as $s_0 = 0$ and $\lambda_0 = \lambda_{\max} \geq \|\mathbf{r}_0\|_2^2 = \|\mathbf{x}_*\|_2^2$. Assume inductively that these hold for k . Note that for any $t \geq 1$, nonnegativity and concavity yield $\rho(ts_*) \leq t\rho(s_*)$. In particular, assuming (21) and applying $\kappa < \sqrt{3/2} - 1$ and $\rho(s_*) \leq c_0$, we get for small enough c_0 that $(1 + \zeta_k)^2 < 2$. Then applying (21) to (19), we get for a constant $C \equiv C(\kappa) > 0$ not depending on c_0 that

$$(1 - C\sqrt{c_0}) \lambda_k s_{k+1} \leq \left(\frac{80}{t(\kappa)^2} + 2 \right) \lambda_k s_*.$$

Then for small enough c_0 ,

$$s_{k+1} \leq (1 - C\sqrt{c_0})^{-1} \frac{82}{t(\kappa)^2} s_* < \frac{90}{t(\kappa)^2} s_*.$$

Applying (21) and this bound to (20), for sufficiently small c_0 , we have

$$\|\mathbf{r}_{k+1}\|_2 \leq \left(1 - \frac{3}{4}t(\kappa) \right) \|\mathbf{r}_k\|_2 + \sqrt{4\lambda_k s_*} \leq \left(\frac{4}{t(\kappa)} - 1 \right) \sqrt{\lambda_k s_*}.$$

Applying $\sqrt{\lambda_k} = \sqrt{\lambda_{k+1}/\gamma} \leq \sqrt{\lambda_{k+1}}(1 - t(\kappa)/4)^{-1}$, we obtain from this

$$\|\mathbf{r}_{k+1}\|_2 \leq \frac{4\sqrt{\lambda_{k+1} s_*}}{t(\kappa)}.$$

This completes the induction and establishes (21) for every k .

The bound (12) follows from (21), the definition of \mathbf{r}_k , and $\lambda_k = \lambda_{\max} \gamma^k$. Since $\mathbf{x}_k, \mathbf{x}_* \in (\delta\mathbb{Z})^p$, for k large enough such that the right side of (12) is less than δ^2 , we must have $\mathbf{x}_k = \mathbf{x}_*$. \square

We now extend this result to provide a robust recovery guarantee in the presence of measurement and discretization error. The proof is an extension of the above argument, which we defer to Appendix A.

Theorem 3.5. *Suppose $\sqrt{\eta} \cdot \mathbf{A}$ satisfies (κ, ρ) -cRIP, where $\kappa \in [0, \sqrt{3/2} - 1)$. Choose tuning parameters γ, λ_{\max} as in Theorem 3.4. Then for some constants $C, C', c > 0$ depending only on κ , the following holds: Let $\mathbf{x} \in (\delta\mathbb{Z})^p$ be any vector satisfying*

$$\rho(s) \leq c, \quad s \equiv \max(\|\nabla\mathbf{x}\|_0, 1).$$

Let D be the maximum vertex degree of G , and define

$$E(\mathbf{x}) = \left(1 + \sqrt{D\rho(s)}\right) \cdot \left(\|\mathbf{x} - \mathbf{x}_*\|_2 + \frac{\|\mathbf{x} - \mathbf{x}_*\|_1}{\sqrt{s}}\right) + \sqrt{\eta} \cdot \|\mathbf{e}\|_2.$$

Suppose $\lambda_{\max} \geq CE(\mathbf{x})^2/s \geq \lambda_{\min}$, and let k_* be the last iterate of Algorithm 1 where $\lambda_{k_*} \geq CE(\mathbf{x})^2/s$. Then $\hat{\mathbf{x}} \equiv \mathbf{x}_{k_*}$ satisfies

$$\|\hat{\mathbf{x}} - \mathbf{x}_*\|_2 \leq C'E(\mathbf{x}).$$

The quantity $E(\mathbf{x})$ above is the combined measurement error and approximation error of \mathbf{x}_* by a discretized piecewise-constant signal \mathbf{x} . For any \mathbf{A} scaled such that it satisfies (κ, ρ) -cRIP with $\eta = 1$, and for G with maximum degree $D \lesssim 1$, we get

$$\|\hat{\mathbf{x}} - \mathbf{x}_*\| \lesssim \|\mathbf{x}_* - \mathbf{x}\|_2 + \frac{\|\mathbf{x}_* - \mathbf{x}\|_1}{\sqrt{s}} + \|\mathbf{e}\|_2.$$

This guarantee is similar to those for compressed sensing of sparse signals in [CRT06b, NT09, BD09]. If \mathbf{x}_* has exact gradient-sparsity $\|\nabla\mathbf{x}_*\|_0 \leq s$, then also $\mathbf{x} \in (\delta\mathbb{Z})^p$ obtained by entrywise rounding to $\delta\mathbb{Z}$ satisfies $\|\nabla\mathbf{x}\|_0 \leq s$. Hence choosing $\delta \ll \|\mathbf{e}\|_2/p$ further ensures

$$\|\hat{\mathbf{x}} - \mathbf{x}_*\| \lesssim \|\mathbf{e}\|_2$$

i.e. the discretization error is negligible in the above bound. The required number of measurements is the same as in Theorem 3.4 for the noiseless setting, which is $n \gtrsim s_* \log(1 + |E|/s_*)$ for i.i.d. Gaussian designs. This is the claim (5) stated in the introduction.

4. SIMULATIONS

We compare $\hat{\mathbf{x}}^{\text{ITALE}}$ using the ℓ_0 edge cost (3) with $\hat{\mathbf{x}}^{\text{TV}}$ minimizing the TV-regularized objective (6), for several signals on the 1-D and 2-D lattice graphs. We used software developed by [BK04] to implement the alpha-expansion sub-routine of Algorithm 2. To minimize the TV-regularized objective (6), we used the generalized lasso path algorithm from [Tib11] in the 1-D examples and the FISTA algorithm from [BT09] in the 2-D examples. All parameters were set as described in Section 2 for ITALE.

4.1. 1-D changepoint signals. We tested ITALE on two simulated signals for the linear chain graph, with different changepoint structures: the “spike” signal depicted in Figures 2 and 3, and the “wave” signal depicted in Figure 4 and 5. The two signals both have $p = 1000$ vertices with $s_* = 9$ break points. The spike signal consists of short segments of length 10 with elevated mean, while the breaks of the wave signal are equally-spaced.

We sampled random Gaussian measurements $A_{ij} \stackrel{iid}{\sim} \mathcal{N}(0, 1)$. The measurement error \mathbf{e} was generated as Gaussian noise $e_k \stackrel{iid}{\sim} \mathcal{N}(0, \sigma^2)$. To provide an intuitive understanding of the tested signal-to-noise, we plot $\mathbf{x}_* + \mathbf{A}^\top \mathbf{e}/n$ in red in Figures 2 to 5, corresponding to two different tested noise levels. Recall that ITALE denoises $\mathbf{a}_{k+1} = \mathbf{x}_* + (\mathbf{I} - \mathbf{A}^\top \mathbf{A}/n)(\mathbf{x}_k - \mathbf{x}_*) + \mathbf{A}^\top \mathbf{e}/n$ in each iteration (corresponding to $\eta = 1/n$ for this normalization of \mathbf{A}), so that $\mathbf{x}_* + \mathbf{A}^\top \mathbf{e}/n$ represents the noisy signal in an ideal setting if $\mathbf{x}_k \equiv \mathbf{x}_*$ is a perfect estimate from the preceding iteration.

Tables 1 and 2 display the root-mean-squared estimation errors

$$\text{RMSE} = \sqrt{\|\hat{\mathbf{x}} - \mathbf{x}_*\|_2^2/p},$$

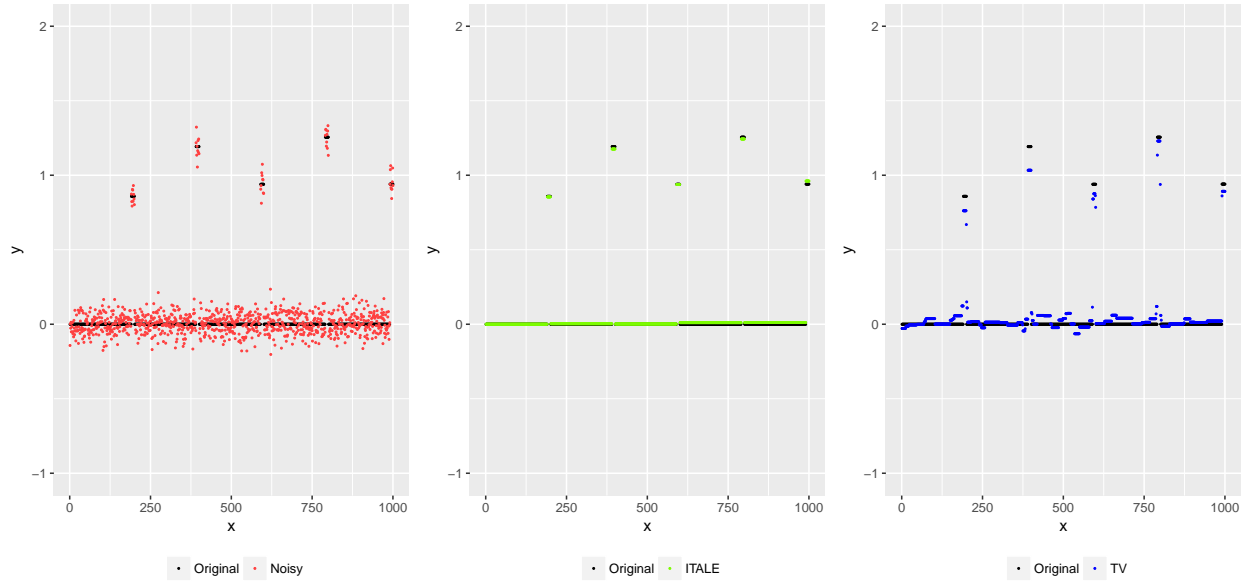


FIGURE 2. Left: True spike signal \mathbf{x}_* (black) and a depiction of $\mathbf{x}_* + \mathbf{A}^\top \mathbf{e}/n$ (red) under low noise $\sigma = 1$ for i.i.d. measurements $A_{ij} \sim \mathcal{N}(0, 1)$ with 15% undersampling. Middle and right: True signal (black), $\hat{\mathbf{x}}^{\text{ITALE}}$ (green), and $\hat{\mathbf{x}}^{\text{TV}}$ (blue) for one simulation.

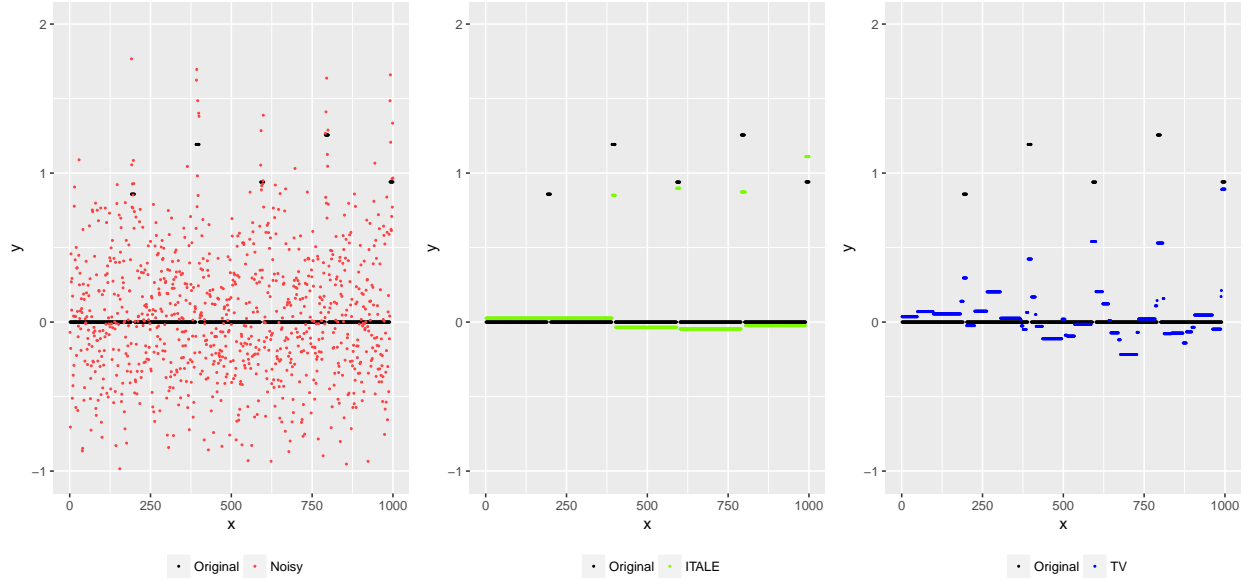


FIGURE 3. Same setting as Figure 2, for noise level $\sigma = 6$.

for undersampling ratio n/p from 10% to 50%, and a range of noise levels σ that yielded RMSE values between 0 and roughly 0.2. Each reported error value is an average across 20 independent simulations. In these results, the iterate k in ITALE and penalty parameter λ in TV were both selected using 5-fold cross-validation. Best-achieved errors over all k and λ are reported in Appendix C, and suggest the same qualitative conclusions. Standard deviations of the RMSE across simulations are also reported in Appendix C.

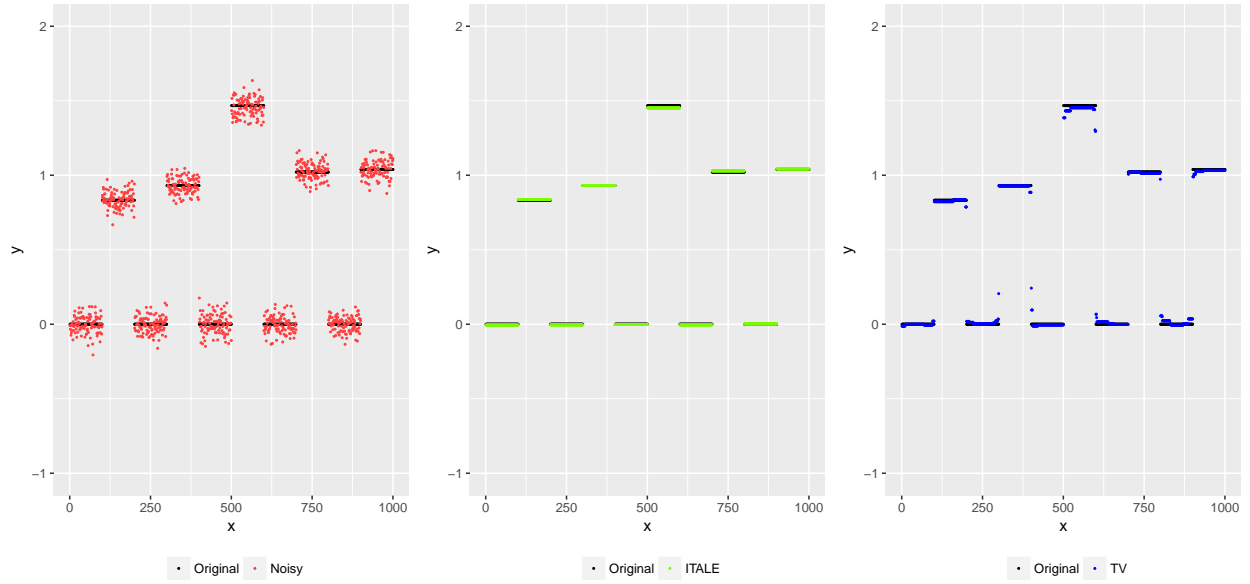


FIGURE 4. Left: True wave signal \mathbf{x}_* (black) and a depiction of $\mathbf{x}_* + \mathbf{A}^\top \mathbf{e}/n$ (red) under low noise $\sigma = 1$ for i.i.d. measurements $A_{ij} \sim \mathcal{N}(0, 1)$ with 15% undersampling. Middle and right: True signal (black), $\hat{\mathbf{x}}^{\text{ITALE}}$ (green), and $\hat{\mathbf{x}}^{\text{TV}}$ (blue) for one simulation.

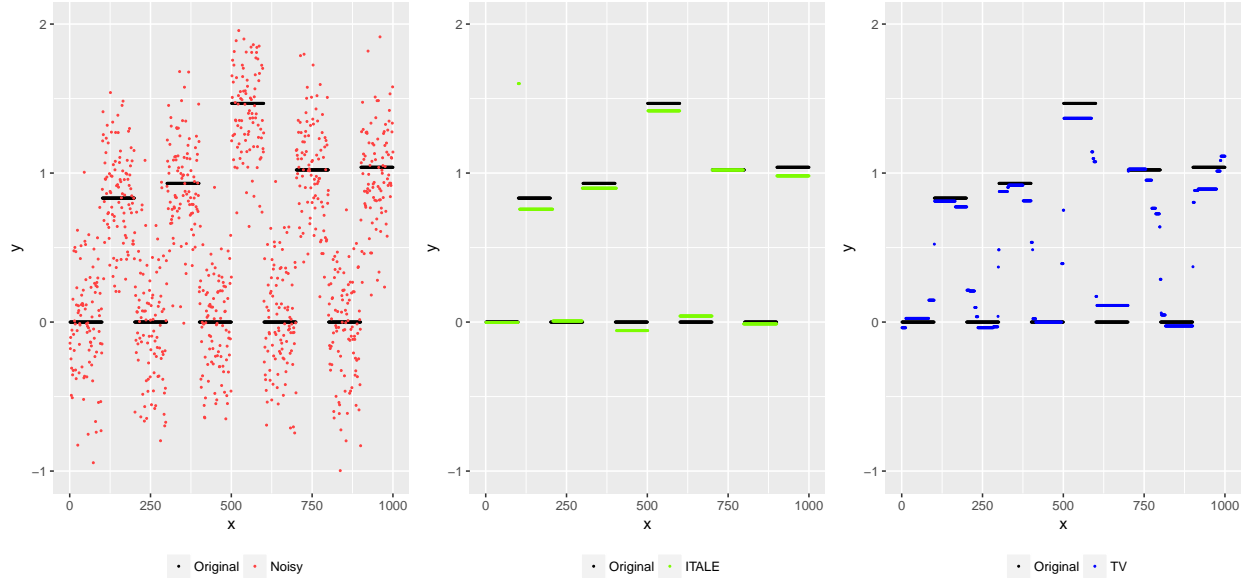


FIGURE 5. Same setting as Figure 4, for noise level $\sigma = 6$.

In the spike example, ITALE yielded lower RMSE in all of the above settings of undersampling and signal-to-noise. Figures 2 and 3 display one instance each of the resulting estimates $\hat{\mathbf{x}}^{\text{ITALE}}$ and $\hat{\mathbf{x}}^{\text{TV}}$ at 15% undersampling, illustrating some of their differences and typical features. Under optimal tuning, $\hat{\mathbf{x}}^{\text{TV}}$ returns an undersmoothed estimate even in a low-noise setting where ITALE can often correctly estimate the changepoint locations. With higher noise, ITALE begins to miss changepoints and oversmooth.

n/p		$\sigma = 0$	$\sigma = 1$	$\sigma = 2$	$\sigma = 3$	$\sigma = 4$	$\sigma = 5$	$\sigma = 6$	$\sigma = 7$
10%	ITALE	0.000	0.014	0.060	0.090	0.144	0.173	0.199	0.216
	TV	0.000	0.047	0.092	0.129	0.160	0.189	0.213	0.228
15%	ITALE	0.000	0.009	0.023	0.049	0.076	0.104	0.133	0.153
	TV	0.000	0.030	0.060	0.088	0.114	0.136	0.158	0.175
20%	ITALE	0.000	0.007	0.015	0.032	0.056	0.076	0.099	0.123
	TV	0.000	0.022	0.045	0.067	0.089	0.109	0.128	0.146
30%	ITALE	0.000	0.006	0.012	0.021	0.031	0.049	0.065	0.079
	TV	0.000	0.017	0.035	0.052	0.070	0.087	0.104	0.120
40%	ITALE	0.000	0.005	0.010	0.015	0.025	0.041	0.051	0.063
	TV	0.000	0.014	0.028	0.043	0.057	0.071	0.085	0.098
50%	ITALE	0.000	0.005	0.010	0.015	0.023	0.033	0.040	0.051
	TV	0.000	0.013	0.026	0.038	0.051	0.064	0.075	0.088

TABLE 1. RMSE for the 1-D spike signal, averaged over 20 simulations.

n/p		$\sigma = 0$	$\sigma = 1$	$\sigma = 2$	$\sigma = 3$	$\sigma = 4$	$\sigma = 5$	$\sigma = 6$	$\sigma = 7$
10%	ITALE	0.036	0.040	0.118	0.150	0.198	0.236	0.262	0.315
	TV	0.000	0.032	0.064	0.093	0.120	0.143	0.168	0.189
15%	ITALE	0.000	0.009	0.025	0.059	0.090	0.111	0.143	0.176
	TV	0.000	0.023	0.046	0.068	0.089	0.109	0.127	0.144
20%	ITALE	0.000	0.007	0.017	0.039	0.061	0.079	0.103	0.121
	TV	0.000	0.019	0.037	0.056	0.074	0.092	0.108	0.124
30%	ITALE	0.000	0.006	0.012	0.019	0.035	0.051	0.065	0.085
	TV	0.000	0.014	0.028	0.042	0.056	0.070	0.084	0.097
40%	ITALE	0.000	0.005	0.011	0.018	0.027	0.037	0.052	0.064
	TV	0.000	0.012	0.024	0.037	0.049	0.061	0.073	0.085
50%	ITALE	0.000	0.005	0.010	0.016	0.024	0.033	0.044	0.055
	TV	0.000	0.011	0.022	0.033	0.043	0.054	0.065	0.075

TABLE 2. RMSE for the 1-D wave signal, averaged over 20 simulations.

In the wave example, with undersampling ranging between 15% and 50%, ITALE yielded lower RMSE at most tested noise levels. Figures 4 and 5 depict two instances of the recovered signals at 15% undersampling. For 10% undersampling, the component $(\mathbf{I} - \mathbf{A}^\top \mathbf{A}/n)(\mathbf{x}_k - \mathbf{x}_*)$ of the effective noise was sufficiently high such that ITALE often did not estimate the true changepoint structure, and TV usually outperformed ITALE in this case. The standard deviations of RMSE reported in Appendix C indicate that the ITALE estimates are a bit more variable than the TV estimates in all tested settings, but particularly so in this 10% undersampling regime.

4.2. 2-D phantom images. Next, we tested ITALE on three 2-D image examples, corresponding to piecewise-constant digital phantom images of varying complexity: the Shepp-Logan digital phantom depicted in Figure 6, a digital brain phantom from [FH94] depicted in Figure 7, and the XCAT chest slice from [GHG⁺17] as previously depicted in Figure 1.

Each image \mathbf{x}_* was normalized to have pixel value in $[0, 1]$. We sampled random Fourier design matrices as specified in (11), fixing the constant $C_0 = 10$ in the weight distribution (10) for this design. This yielded the best recovery across several tested values for both ITALE and TV. The measurement error \mathbf{e} was generated as Gaussian noise $e_k \stackrel{iid}{\sim} \mathcal{N}(0, \sigma^2)$, applied to the measurements $\mathcal{F}_{(i,j)}^* \mathbf{x}_* / \sqrt{\nu(i,j)}$ before the $1/\sqrt{n}$ normalization. Tables 3, 4, and 5 display the RMSE of the

n/p		$\sigma = 0$	$\sigma = 4$	$\sigma = 8$	$\sigma = 12$	$\sigma = 16$	$\sigma = 20$	$\sigma = 24$	$\sigma = 28$
10%	ITALE	0.001	0.007	0.012	0.018	0.023	0.039	0.047	0.072
	TV	0.005	0.011	0.021	0.031	0.040	0.051	0.057	0.062
15%	ITALE	0.000	0.003	0.011	0.014	0.017	0.027	0.035	0.044
	TV	0.001	0.008	0.016	0.026	0.030	0.038	0.049	0.053
20%	ITALE	0.000	0.003	0.008	0.012	0.017	0.024	0.027	0.036
	TV	0.000	0.007	0.014	0.021	0.027	0.032	0.039	0.045
30%	ITALE	0.000	0.002	0.005	0.011	0.013	0.015	0.018	0.026
	TV	0.000	0.006	0.012	0.017	0.023	0.027	0.032	0.036
40%	ITALE	0.000	0.001	0.005	0.010	0.011	0.013	0.017	0.018
	TV	0.000	0.005	0.010	0.015	0.019	0.023	0.028	0.032
50%	ITALE	0.000	0.001	0.004	0.008	0.011	0.013	0.013	0.015
	TV	0.000	0.005	0.009	0.013	0.017	0.021	0.025	0.029

TABLE 3. RMSE for the Shepp-Logan phantom

n/p		$\sigma = 0$	$\sigma = 8$	$\sigma = 16$	$\sigma = 24$	$\sigma = 32$	$\sigma = 40$	$\sigma = 48$	$\sigma = 56$
10%	ITALE	0.003	0.002	0.010	0.028	0.043	0.060	0.080	0.096
	TV	0.002	0.014	0.028	0.042	0.054	0.064	0.078	0.085
15%	ITALE	0.000	0.001	0.007	0.019	0.030	0.044	0.059	0.075
	TV	0.001	0.011	0.022	0.032	0.043	0.053	0.063	0.074
20%	ITALE	0.000	0.001	0.005	0.012	0.025	0.036	0.047	0.056
	TV	0.000	0.009	0.019	0.028	0.038	0.046	0.056	0.061
30%	ITALE	0.000	0.001	0.002	0.007	0.014	0.025	0.033	0.044
	TV	0.000	0.007	0.016	0.023	0.030	0.038	0.046	0.053
40%	ITALE	0.000	0.000	0.002	0.006	0.010	0.021	0.027	0.037
	TV	0.000	0.007	0.013	0.019	0.026	0.032	0.039	0.043
50%	ITALE	0.000	0.001	0.002	0.005	0.007	0.016	0.022	0.029
	TV	0.000	0.006	0.011	0.018	0.023	0.029	0.036	0.040

TABLE 4. RMSE for the brain phantom

n/p		$\sigma = 0$	$\sigma = 4$	$\sigma = 8$	$\sigma = 12$	$\sigma = 16$	$\sigma = 20$	$\sigma = 24$	$\sigma = 28$
10%	ITALE	0.063	0.064	0.068	0.078	0.084	0.092	0.099	0.106
	TV	0.009	0.019	0.032	0.044	0.054	0.061	0.068	0.072
15%	ITALE	0.002	0.007	0.025	0.036	0.048	0.070	0.079	0.085
	TV	0.005	0.014	0.024	0.035	0.043	0.050	0.056	0.061
20%	ITALE	0.002	0.005	0.014	0.023	0.033	0.045	0.052	0.079
	TV	0.002	0.011	0.020	0.028	0.037	0.043	0.049	0.056
30%	ITALE	0.002	0.004	0.011	0.018	0.025	0.033	0.041	0.049
	TV	0.002	0.008	0.016	0.023	0.030	0.036	0.042	0.046
40%	ITALE	0.002	0.003	0.009	0.014	0.020	0.026	0.033	0.038
	TV	0.001	0.007	0.014	0.020	0.025	0.031	0.036	0.041
50%	ITALE	0.002	0.003	0.008	0.013	0.018	0.024	0.029	0.033
	TV	0.001	0.006	0.012	0.018	0.024	0.029	0.033	0.038

TABLE 5. RMSE for the XCAT chest slice phantom

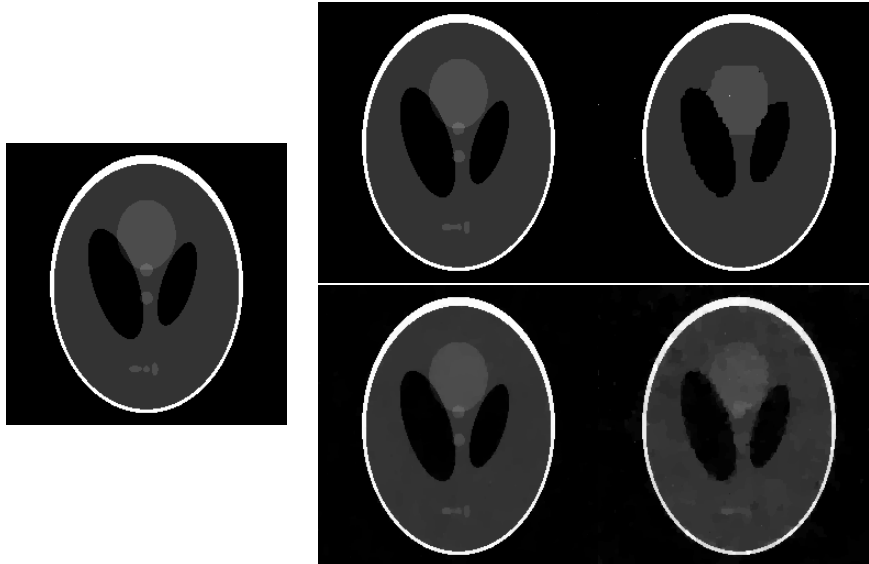


FIGURE 6. Left: Original Shepp-Logan phantom. Top row: $\hat{\mathbf{x}}^{\text{ITALE}}$ from 15% undersampled and reweighted Fourier measurements, in low noise ($\sigma = 4$, left) and medium noise ($\sigma = 16$, right) settings. Bottom row: $\hat{\mathbf{x}}^{\text{TV}}$ for the same measurements.

estimates $\hat{\mathbf{x}}^{\text{ITALE}}$ and $\hat{\mathbf{x}}^{\text{TV}}$ for a single simulation, with tuning parameters selected by 5-fold cross-validation. Best-achieved errors are reported in Appendix C.

For the simpler Logan-Shepp and brain phantom images, which exhibit stronger gradient-sparsity, ITALE yielded lower RMSE in nearly all tested undersampling and signal-to-noise regimes. For the XCAT chest phantom, with undersampling ranging between 15% and 50%, ITALE yielded lower RMSE at a range of tested noise levels, and in particular for those settings of higher signal-to-noise. With 10% undersampling for the XCAT phantom, ITALE was not able to recover some details of the XCAT image even with no measurement noise, and RMSE was higher than TV at all tested noise levels. Results of Appendix C indicate that this is partially due to sub-optimal selection of the tuning parameter using 5-fold cross-validation, caused by the further reduction of undersampling from 10% to 8% in the size of the training data in each fold.

Examples of recovered signals $\hat{\mathbf{x}}^{\text{ITALE}}$ and $\hat{\mathbf{x}}^{\text{TV}}$ are depicted for the Shepp-Logan and brain phantoms in Figures 6 and 7, at 15% and 20% undersampling for two low-noise and medium-noise settings. The qualitative comparisons are similar to those in the 1-D simulations, and to those previously depicted for the XCAT chest slice in Figure 1: As measurement noise increases, ITALE begins to lose finer details, while TV begins to yield an undersmoothed and blotchy image. These observations are also similar to previous comparisons that have been made for algorithms oriented towards ℓ_0 versus TV regularization for direct measurements $\mathbf{A} = \mathbf{I}$, in [XLXJ11, FG18, KG19].

5. CONCLUSION

We have studied recovery of piecewise-constant signals over arbitrary graphs from noisy linear measurements. We have proposed an iterative algorithm, ITALE, to minimize an ℓ_0 -edge-penalized least-squares objective. Under a cut-restricted isometry property for the measurement design, we have established global recovery guarantees for the estimated signal, in noisy and noiseless settings.

In the field of compressed sensing, for signals exhibiting sparsity in an orthonormal basis, ℓ_1 -regularization [Don06, CRT06b, CRT06a] and discrete iterative algorithms [TG07, NT09, BD09] constitute two major approaches for signal recovery. It has been observed that for recovering



FIGURE 7. Left: Original brain phantom. Top row: $\hat{\mathbf{x}}^{\text{ITALE}}$ from 20% undersampled reweighted Fourier measurements, in low noise ($\sigma = 16$, left) and medium noise ($\sigma = 40$, right) settings. Bottom row: $\hat{\mathbf{x}}^{\text{TV}}$ for the same measurements.

piecewise-constant signals, regularizing the signal gradient in a sparse analysis framework can yield better empirical recovery than regularizing signal coefficients in such a basis. Whereas ℓ_1 -regularization extends naturally to the sparse analysis setting, iterative algorithms have received less attention. By applying the alpha-expansion idea for MAP estimation in discrete Markov random fields, ITALE provides a computationally tractable approach for “iterative thresholding” recovery of gradient-sparse signals, with provable recovery guarantees.

In contrast to sparse signal recovery over an orthonormal basis, the comparison of ℓ_1 versus ℓ_0 regularization for gradient-based sparsity is graph-dependent. Using an ℓ_0 -based approach, we establish signal recovery guarantees on the 1-D and 2-D lattice graphs with numbers of measurements optimal up to a constant factor, which were not previously available for TV-regularization. This difference is closely connected to slow and fast rates of convergence for lasso and best-subset regression for correlated regression designs [BRvdGZ13, ZWJ14, DHL17]. ITALE provides a polynomial-time approach for ℓ_0 -regularization in a special graph-based setting, and we believe it is an interesting question whether similar algorithmic ideas may be applicable to other classes of sparse regression problems.

APPENDIX A. PROOF OF ROBUST RECOVERY GUARANTEE

In this appendix, we prove Theorem 3.5 providing the estimation guarantee under approximate gradient-sparsity and discretization and measurement error.

Lemma A.1. *Suppose G has maximum vertex degree D , and $\mathbf{A} \in \mathbb{R}^{n \times p}$ satisfies (κ, ρ) -cRIP. Then for any $\mathbf{u} \in \mathbb{R}^p$ and $s \geq 1$,*

$$\|\mathbf{A}\mathbf{u}\|_2 \leq \left(1 + \kappa + \sqrt{D\rho(s)}\right) \cdot \left(\|\mathbf{u}\|_2 + \frac{\|\mathbf{u}\|_1}{\sqrt{s}}\right).$$

Proof. Let $T_1 \subseteq \{1, \dots, p\}$ be the s indices corresponding to the s entries of \mathbf{u} with largest magnitude (breaking ties arbitrarily). Let $T_2 \subseteq \{1, \dots, p\} \setminus T_1$ be the s indices corresponding to the next s entries of \mathbf{u} with largest magnitude, and define sequentially T_3, T_4, \dots, T_m for $m = \lceil p/s \rceil$ in this way. Denote by $\mathbf{u}_{T_i} \in \mathbb{R}^p$ the vector with j^{th} entry equal to u_j if $j \in T_i$, or 0 otherwise. Then $\|\nabla \mathbf{u}_{T_i}\|_0 \leq Ds$ for each i . Applying the triangle inequality and cRIP condition for \mathbf{A} ,

$$\|\mathbf{A}\mathbf{u}\|_2 \leq \sum_{i=1}^m \|\mathbf{A}\mathbf{u}_{T_i}\|_2 \leq \left(1 + \kappa + \sqrt{\rho(Ds)}\right) \cdot \sum_{i=1}^m \|\mathbf{u}_{T_i}\|_2.$$

For $i \geq 2$, we have $\|\mathbf{u}_{T_{i+1}}\|_\infty \leq \|\mathbf{u}_{T_i}\|_1/s$ by construction, so

$$\|\mathbf{u}_{T_{i+1}}\|_2 \leq \sqrt{s} \cdot \frac{\|\mathbf{u}_{T_i}\|_1}{s} = \frac{\|\mathbf{u}_{T_i}\|_1}{\sqrt{s}}.$$

Applying this for $i \geq 2$, and the bound $\|\mathbf{u}_{T_1}\|_2 \leq \|\mathbf{u}\|_2$ for $i = 1$,

$$\|\mathbf{A}\mathbf{u}\|_2 \leq \left(1 + \kappa + \sqrt{\rho(Ds)}\right) \cdot \left(\|\mathbf{u}\|_2 + \frac{\sum_{i=1}^{m-1} \|\mathbf{u}_{T_i}\|_1}{\sqrt{s}}\right) \leq \left(1 + \kappa + \sqrt{\rho(Ds)}\right) \left(\|\mathbf{u}\|_2 + \frac{\|\mathbf{u}\|_1}{\sqrt{s}}\right).$$

Finally, we have $(\rho(Ds) - \rho(0))/Ds \leq (\rho(s) - \rho(0))/s$ by the concavity of ρ , and hence $\rho(Ds) \leq D\rho(s)$ since $\rho(0) \geq 0$. \square

Proof of Theorem 3.5. Write $\mathbf{y} = \mathbf{A}\mathbf{x} + \tilde{\mathbf{e}}$ where $\tilde{\mathbf{e}} = \mathbf{A}(\mathbf{x}_* - \mathbf{x}) + \mathbf{e}$. Denote

$$s = \max(\|\nabla \mathbf{x}\|_0, 1), \quad s_k = \|\nabla \mathbf{x}_k\|_0, \quad \mathbf{r}_k = \mathbf{x}_k - \mathbf{x}.$$

As in the proof of Theorem 3.4, consider the partitions of $\{1, \dots, p\}$ induced by the piecewise-constant structures of \mathbf{x}_k , \mathbf{x}_{k+1} , and \mathbf{x} , let \mathcal{S} be their common refinement, and let \mathbf{P} be the orthogonal projection onto the subspace of signals taking constant value over each set in \mathcal{S} . Applying

$$\mathbf{a}_{k+1} = \mathbf{x}_k - \eta \mathbf{A}^\top (\mathbf{A}\mathbf{x}_k - \mathbf{y}) = \mathbf{x}_k - \eta \mathbf{A}^\top \mathbf{A}\mathbf{r}_k + \eta \mathbf{A}^\top \tilde{\mathbf{e}},$$

the same arguments as leading to (15) yield

$$\left(\|\mathbf{r}_{k+1}\|_2 - \|\mathbf{r}_k - \eta \mathbf{P}\mathbf{A}^\top \mathbf{A}\mathbf{r}_k + \eta \mathbf{P}\mathbf{A}^\top \tilde{\mathbf{e}}\|_2\right)_+^2 \leq \|\mathbf{r}_k - \eta \mathbf{P}\mathbf{A}^\top \mathbf{A}\mathbf{r}_k + \eta \mathbf{P}\mathbf{A}^\top \tilde{\mathbf{e}}\|_2^2 + \lambda_k(4s - 2s_{k+1}). \quad (22)$$

Set $S_k = s + s_k + s_{k+1}$, $T_k = s + s_k$, and

$$\tau_k = \kappa + \sqrt{\rho(S_k)}, \quad \zeta_k = \kappa + \sqrt{\rho(T_k)}, \quad d_k = 2(1 + \kappa)\sqrt{\rho(T_k)} + \rho(T_k).$$

Then we obtain analogously to (16) and (19) that

$$\lambda_k s_{k+1} \leq \|\mathbf{r}_k\|_2^2 + 2\|\sqrt{\eta}\mathbf{A}\mathbf{P}\|_{\text{op}}^2 \cdot \|\sqrt{\eta}\mathbf{A}\mathbf{r}_k\|_2^2 + 2\|\eta\mathbf{P}\mathbf{A}^\top \tilde{\mathbf{e}}\|_2^2 + 2\lambda_k s,$$

and hence

$$(\lambda_k - 2(1 + \zeta_k)^2 d_k \|\mathbf{r}_k\|_2^2/s) \cdot s_{k+1} \leq (1 + 2(1 + \zeta_k)^4) \cdot \|\mathbf{r}_k\|_2^2 + 2\|\eta\mathbf{P}\mathbf{A}^\top \tilde{\mathbf{e}}\|_2^2 + 2\lambda_k s. \quad (23)$$

Similarly, taking the square-root in (22), we obtain analogously to (20) that

$$\|\mathbf{r}_{k+1}\|_2 \leq \left[1 - t(\kappa) + 4\sqrt{\rho(S_k)} + 2\rho(S_k)\right] \cdot \|\mathbf{r}_k\|_2 + 2\|\eta\mathbf{P}\mathbf{A}^\top \tilde{\mathbf{e}}\|_2 + \sqrt{4\lambda_k s}. \quad (24)$$

Recalling the bound $\|\sqrt{\eta}\mathbf{A}\mathbf{P}\|_{\text{op}} \leq 1 + \tau_k$ from (17), we have

$$\|\eta\mathbf{P}\mathbf{A}^\top \tilde{\mathbf{e}}\|_2 \leq (1 + \tau_k)(\|\sqrt{\eta}\mathbf{A}(\mathbf{x}_* - \mathbf{x})\|_2 + \|\sqrt{\eta} \cdot \mathbf{e}\|_2).$$

Bounding $\|\sqrt{\eta}\mathbf{A}(\mathbf{x}_* - \mathbf{x})\|_2$ using the given cRIP condition and Lemma A.1 with the choice $s = \max(\|\nabla \mathbf{x}\|_0, 1)$ as above, we get for a constant $c_1 > 0$ that

$$\|\eta\mathbf{P}\mathbf{A}^\top \tilde{\mathbf{e}}\|_2 \leq (1 + \tau_k)c_1 E(\mathbf{x}).$$

Applying this and the bound $(1 + \tau_k)^2 \leq (1 + \zeta_k)^2 + d_k s_{k+1}/s$ from (18) to (23), we get

$$(\lambda_k - 2e_k d_k/s) \cdot s_{k+1} \leq \|\mathbf{r}_k\|_2^2 + 2e_k(1 + \zeta_k)^2 + 2\lambda_k s \quad (25)$$

for the quantity

$$e_k = (1 + \zeta_k)^2 \|\mathbf{r}_k\|_2^2 + c_1^2 E(\mathbf{x})^2.$$

Also, applying this to (24), we get

$$\|\mathbf{r}_{k+1}\|_2 \leq \left[1 - t(\kappa) + 4\sqrt{\rho(S_k)} + 2\rho(S_k)\right] \cdot \|\mathbf{r}_k\|_2 + 2(1 + \tau_k)c_1 E(\mathbf{x}) + \sqrt{4\lambda_k s}. \quad (26)$$

We now claim by induction on k that if $\rho(s) \leq c_0$ and $\lambda_k \geq C_0 E(\mathbf{x})^2/s$ for every $k \leq k_*$, where $C_0 > 0$ is sufficiently large and $c_0 > 0$ is sufficiently small, then for every $k \leq k_*$ we have

$$s_k \leq \frac{200}{t(\kappa)^2} s, \quad \|\mathbf{r}_k\|_2 \leq \frac{4\sqrt{\lambda_k s}}{t(\kappa)}. \quad (27)$$

For $k = 0$, these are satisfied as $s_0 = 0$ and $\lambda_0 = \lambda_{\max} \geq \|\mathbf{r}_0\|_2^2$. Assume inductively that these hold for k , where $k \leq k_* - 1$. Then for small enough c_0 , we have $(1 + \zeta_k)^2 < 2$ and hence

$$e_k \leq \frac{32\lambda_k s}{t(\kappa)^2} + c_1^2 E(\mathbf{x})^2.$$

Also, $d_k \leq C\sqrt{c_0}$ for a constant $C \equiv C(\kappa) > 0$ independent of c_0 . Then for C_0 large enough and c_0 small enough, we obtain from (25) and the condition $\lambda_k \geq C_0 E(\mathbf{x})^2/s$ that

$$\frac{3}{4}\lambda_k s_{k+1} \leq \|\mathbf{r}_k\|_2^2 + 4e_k + 2\lambda_k s \leq \frac{146\lambda_k s}{t(\kappa)^2} + 4c_1^2 E(\mathbf{x})^2 < \frac{150\lambda_k s}{t(\kappa)^2}.$$

This gives the bound

$$s_{k+1} \leq \frac{200}{t(\kappa)^2} s.$$

Then applying (27) and this bound to (26), again for $\rho(s) \leq c_0$ and $\lambda_k s \geq C_0 E(\mathbf{x})^2$ with C_0 sufficiently large and c_0 sufficiently small, we get

$$\|\mathbf{r}_{k+1}\|_2 \leq \left(1 - \frac{4}{5}t(\kappa)\right) \|\mathbf{r}_k\|_2 + 6c_1 E(\mathbf{x}) + \sqrt{4\lambda_k s} < \left(\frac{4}{t(\kappa)} - 1\right) \sqrt{\lambda_k s}.$$

Applying $\sqrt{\lambda_k} = \sqrt{\lambda_{k+1}/\gamma} \leq \sqrt{\lambda_{k+1}}(1 - t(\kappa)/4)^{-1}$, we obtain

$$\|\mathbf{r}_{k+1}\|_2 \leq \frac{4\sqrt{\lambda_{k+1} s}}{t(\kappa)},$$

completing the induction. This establishes (27) for every $k \leq k_*$, provided $\lambda_{k_*} \geq C_0 E(\mathbf{x})^2/s$. In particular, at the iterate k_* , we have $\lambda_{k_*} s \asymp E(\mathbf{x})^2$ and hence $\|\mathbf{r}_{k_*}\|_2 \lesssim E(\mathbf{x})$. \square

APPENDIX B. PROOFS OF CUT-RESTRICTED ISOMETRY PROPERTY

In this appendix, we prove Propositions 3.2 and 3.3 establishing cRIP for the sub-Gaussian and weighted 2D-Fourier designs.

Proof of Proposition 3.2. First fix $s \in \{1, \dots, |E|\}$. For each partition \mathcal{S} of $V = \{1, \dots, p\}$ with $|\partial\mathcal{S}| = s$, let $\mathbf{P}_{\mathcal{S}} : \mathbb{R}^p \rightarrow K_{\mathcal{S}}$ be the associated orthogonal projection onto the subspace $K_{\mathcal{S}}$ of signals which are constant on each set in \mathcal{S} . Note that the dimension of $K_{\mathcal{S}}$ is the number of sets in \mathcal{S} , which is at most $s + 1$ because G is a connected graph. Write $\mathbf{P}_{\mathcal{S}} = \mathbf{Q}_{\mathcal{S}}\mathbf{Q}_{\mathcal{S}}^{\top}$, where $\mathbf{Q}_{\mathcal{S}}$ has orthonormal columns spanning $K_{\mathcal{S}}$. Then $\mathbf{A}\mathbf{Q}_{\mathcal{S}}$ still has independent rows $\mathbf{a}_i^{\top}\mathbf{Q}_{\mathcal{S}}/\sqrt{n}$, where

$\|\mathbf{a}_i^\top \mathbf{Q}_S\|_{\psi_2} \leq K$ and $\text{Cov}[\mathbf{a}_i^\top \mathbf{Q}_S] = \mathbf{Q}_S^\top \Sigma \mathbf{Q}_S$. Applying [Ver10, Eq. (5.25)] to $\mathbf{A}\mathbf{Q}_S$, for any $t > 0$ and some constants $C, c > 0$ depending only on K ,

$$\mathbb{P} \left[\|\mathbf{Q}_S^\top \mathbf{A}^\top \mathbf{A} \mathbf{Q}_S - \mathbf{Q}_S^\top \Sigma \mathbf{Q}_S\|_{\text{op}} \geq \max(\delta, \delta^2) \right] \leq 2e^{-ct^2}, \quad \delta \equiv \frac{C\sqrt{s+t}}{\sqrt{n}}.$$

Let $g(s) = s \log(1 + |E|/s)$, and note that there are at most $\binom{|E|}{s} \leq e^{g(s)}$ partitions \mathcal{S} where $|\partial \mathcal{S}| = s$. Taking a union bound over \mathcal{S} , and noting that any \mathbf{u} with $\|\nabla \mathbf{u}\|_0 = s$ may be represented as $\mathbf{u} = \mathbf{Q}_S \mathbf{v}$ for some such \mathcal{S} , this yields

$$\mathbb{P} \left[\sup_{\mathbf{u} \in \mathbb{R}^p: \|\mathbf{u}\|_2=1, \|\nabla \mathbf{u}\|_0=s} |\mathbf{u}^\top \mathbf{A}^\top \mathbf{A} \mathbf{u} - \mathbf{u}^\top \Sigma \mathbf{u}| \geq \max(\delta, \delta^2) \right] \leq 2e^{g(s)-ct^2}.$$

When $\|\mathbf{u}\|_2 = 1$ and $|\mathbf{u}^\top \mathbf{A}^\top \mathbf{A} \mathbf{u} - \mathbf{u}^\top \Sigma \mathbf{u}| \leq \max(\delta, \delta^2)$, we have

$$\|\mathbf{A}\mathbf{u}\|_2 \leq \sqrt{\mathbf{u}^\top \Sigma \mathbf{u} + \max(\delta, \delta^2)} \leq \sqrt{(1 + \kappa)^2 + \max(\delta, \delta^2)} \leq 1 + \kappa + \delta.$$

We also have

$$\|\mathbf{A}\mathbf{u}\|_2 \geq \sqrt{(\mathbf{u}^\top \Sigma \mathbf{u} - \max(\delta, \delta^2))_+} \geq \sqrt{((1 - \kappa)^2 - \max(\delta, \delta^2))_+} \geq 1 - \kappa - \frac{\delta}{1 - \kappa},$$

where the last inequality is trivial for $\delta \geq (1 - \kappa)^2$ and may be checked for $\delta \leq (1 - \kappa)^2$ by squaring both sides and applying $\max(\delta, \delta^2) = \delta$ in this case. Then, for any k and some constants $C_0, C_1 > 0$ depending on k , setting $t = \sqrt{C_0 g(s)}$ and applying $g(s) \geq g(1) = \log(1 + |E|)$, we get

$$\mathbb{P} \left[\sup_{\mathbf{u} \in \mathbb{R}^p: \|\mathbf{u}\|_2=1, \|\nabla \mathbf{u}\|_0=s} \left| \|\mathbf{A}\mathbf{u}\|_2 - 1 \right| \leq \kappa + \sqrt{\frac{C_1 g(s)}{n}} \right] \leq |E|^{-k-1}.$$

Taking a union bound over $s = 1, \dots, |E|$ and applying scale invariance of the cRIP condition to $\|\mathbf{u}\|_2$ concludes the proof. \square

Next, we establish Proposition 3.3 on the Fourier design.

Lemma B.1. *Let $p = N_1 N_2$, let $S \times T \subset \{1, \dots, N_1\} \times \{1, \dots, N_2\}$ be any connected rectangle, and let $\mathcal{F} \in \mathbb{C}^{p \times p}$ be the 2-D discrete Fourier matrix defined in Section 3.1. Then for any $(i, j) \in \{1, \dots, N_1\} \times \{1, \dots, N_2\}$,*

$$\left| \sum_{(i', j') \in S \times T} \mathcal{F}_{(i, j), (i', j')} \right| \leq \sqrt{\frac{|S|}{1 + \min(i-1, N_1 - i + 1)}} \cdot \sqrt{\frac{|T|}{1 + \min(j-1, N_2 - j + 1)}}.$$

Proof. Since

$$\left| \sum_{(i', j') \in S \times T} \mathcal{F}_{(i, j), (i', j')} \right| = \left| \sum_{i' \in S} \mathcal{F}_{i, i'}^1 \cdot \sum_{j' \in T} \mathcal{F}_{j, j'}^2 \right|$$

for the 1-D Fourier matrices $\mathcal{F}^1 \in \mathbb{C}^{N_1 \times N_1}$ and $\mathcal{F}^2 \in \mathbb{C}^{N_2 \times N_2}$, it suffices to show

$$\left| \sum_{k \in S} \mathcal{F}_{ik}^1 \right| \leq \sqrt{\frac{|S|}{1 + \min(i-1, N_1 - i + 1)}}.$$

For this, denote the elements of S as $\{k_1 + 1, \dots, k_1 + |S|\}$, and write

$$\left| \sum_{k \in S} \mathcal{F}_{ik}^1 \right| = \left| \frac{1}{\sqrt{N_1}} \sum_{t=0}^{|S|-1} e^{2\pi i \cdot \frac{(i-1)k_1}{N_1}} \cdot e^{2\pi i \cdot \frac{(i-1)t}{N_1}} \right| = \frac{1}{\sqrt{N_1}} \left| \sum_{t=0}^{|S|-1} e^{2\pi i \cdot \frac{(i-1)t}{N_1}} \right|.$$

This is at most $|S|/\sqrt{N_1}$, which implies the bound for $i = 1$. For $i \geq 2$, apply further

$$|1 - e^{2\pi it}| \geq 4 \min(t, 1 - t)$$

for $t \in [0, 1]$. Then summing the geometric series, we also have

$$\begin{aligned} \left| \sum_{k \in S} \mathcal{F}_{ik}^1 \right| &= \frac{1}{\sqrt{N_1}} \left| 1 - e^{2\pi i \frac{(i-1)|S|}{N_1}} \right| \cdot \left| 1 - e^{2\pi i \frac{(i-1)}{N_1}} \right|^{-1} \\ &\leq \frac{\sqrt{N_1}}{2 \min(i-1, N_1 - i + 1)} \leq \frac{\sqrt{N_1}}{1 + \min(i-1, N_1 - i + 1)}. \end{aligned}$$

The result follows from combining this with the previous upper bound bound $|S|/\sqrt{N_1}$, using $\min(a, b) \leq \sqrt{ab}$. \square

Lemma B.2. *Let $p = N_1 N_2$, where N_1, N_2 are powers of 2 and $1/K \leq N_1/N_2 \leq K$ for a constant $K > 0$. Let G be the 2-D lattice graph of size $N_1 \times N_2$. For $\mathbf{x} \in \mathbb{C}^p$, let $|c_{(1)}(\mathbf{x})| \geq \dots \geq |c_{(p)}(\mathbf{x})|$ be the ordered magnitudes of the coefficients of \mathbf{x} in the bivariate Haar wavelet basis. If \mathbf{x} is centered to have mean entry 0, then for a constant $C \equiv C(K) > 0$ and each $k = 1, \dots, p$,*

$$|c_{(k)}(\mathbf{x})| \leq C \cdot \frac{\|\nabla \mathbf{x}\|_1}{k}$$

where ∇ is the discrete gradient operator on G .

Proof. See [NW13b, Proposition 8] for the case $N_1 = N_2$. For $N_1 < N_2$, we may apply this result to the ‘‘stretched’’ image where each original vertex value is copied to N_2/N_1 consecutive values in a vertical strip. This stretching changes $\|\nabla \mathbf{x}\|_1$ and each original bivariate Haar wavelet coefficient by at most a constant factor, and introduces $N_2^2 - N_1 N_2$ new Haar wavelet coefficients which are identically 0. Thus the result still holds in this case, and similarly for $N_1 > N_2$. \square

Proof of Proposition 3.3. We follow closely the ideas of [RV08, Theorem 3.3].

For each partition $\mathcal{S} = (S_1, \dots, S_k)$ of G into k connected pieces, let $K_{\mathcal{S}} \subset \mathbb{C}^p$ be the k -dimensional subspace of vectors which take a constant value over each set of \mathcal{S} . For each sparsity level $s \geq 1$, define

$$K_s = \bigcup_{\mathcal{S}: |\partial \mathcal{S}| \leq s} \{\mathbf{x} \in K_{\mathcal{S}} : \|\mathbf{x}\|_2 \leq 1\}, \quad \kappa_s = \sup_{\mathbf{x} \in K_s} |\mathbf{x}^*(\mathbf{A}^* \mathbf{A} - \mathbf{I})\mathbf{x}|.$$

It suffices to show, with the stated probability and form of ρ , that

$$\kappa_s \leq 2\sqrt{\rho(s)} + \rho(s)$$

holds simultaneously for all $s = 1, \dots, |E|$.

We first control $\mathbb{E}[\kappa_s]$ using a metric entropy argument: Letting \mathbf{A}_r^* be row r of \mathbf{A} ,

$$n \cdot \mathbb{E}[\mathbf{A}_r \mathbf{A}_r^*] = \mathbb{E} \left[\frac{\mathcal{F}_{(i_r, j_r)} \mathcal{F}_{(i_r, j_r)}^*}{\nu(i_r, j_r)} \right] = \sum_{(i, j)} \mathcal{F}_{(i, j)} \mathcal{F}_{(i, j)}^* = \mathbf{I}.$$

So

$$\kappa_s = \sup_{\mathbf{x} \in K_s} \cdot \left| \sum_{r=1}^n (|\mathbf{A}_r^* \mathbf{x}|^2 - \mathbb{E}|\mathbf{A}_r^* \mathbf{x}|^2) \right|.$$

Applying Gaussian symmetrization,

$$\mathbb{E}[\kappa_s] \leq C \mathbb{E} \sup_{\mathbf{x} \in K_s} \left| \sum_{r=1}^n g_r |\mathbf{A}_r^* \mathbf{x}|^2 \right|$$

for a constant $C > 0$ and $g_1, \dots, g_n \stackrel{iid}{\sim} \mathcal{N}(0, 1)$ independent of \mathbf{A} .

Condition on \mathbf{A} , and define by $E(\mathbf{A})$ the right side above with the expectation taken only over g_1, \dots, g_n . Introducing the pseudo-metric

$$d(\mathbf{x}, \mathbf{y}) = \sqrt{\sum_{r=1}^n (|\mathbf{A}_r^* \mathbf{x}|^2 - |\mathbf{A}_r^* \mathbf{y}|^2)^2},$$

Dudley's inequality yields

$$E(\mathbf{A}) \leq C \int_0^\infty \sqrt{\log N(K_s, d, u)} du$$

where $N(K_s, d, u)$ is the covering number of K_s by balls of radius u in the metric d . For $\mathbf{x}, \mathbf{y} \in K_s$,

$$\begin{aligned} d(\mathbf{x}, \mathbf{y}) &\leq \sqrt{\sum_{r=1}^n |\mathbf{A}_r^* \mathbf{x} + \mathbf{A}_r^* \mathbf{y}|^2 |\mathbf{A}_r^* \mathbf{x} - \mathbf{A}_r^* \mathbf{y}|^2} \\ &\leq \sqrt{2 \sup_{\mathbf{z} \in K_s} \sum_{r=1}^n |\mathbf{A}_r^* \mathbf{z}|^2 \cdot \max_{r=1}^n |\mathbf{A}_r^* \mathbf{x} - \mathbf{A}_r^* \mathbf{y}|} = R(\mathbf{A}) \cdot \|\mathbf{x} - \mathbf{y}\|_{\mathbf{A}}, \end{aligned}$$

where

$$R(\mathbf{A})^2 = \sup_{\mathbf{z} \in K_s} \mathbf{z}^* \mathbf{A}^* \mathbf{A} \mathbf{z}, \quad \|\mathbf{x}\|_{\mathbf{A}} = \sqrt{2} \cdot \max_{r=1}^n |\mathbf{A}_r^* \mathbf{x}|.$$

Applying this bound and a change-of-variables $v = u/R(\mathbf{A})$,

$$E(\mathbf{A}) \leq CR(\mathbf{A}) \int_0^\infty \sqrt{\log N(K_s, \|\cdot\|_{\mathbf{A}}, v)} dv. \quad (28)$$

The pseudo-norm $\|\cdot\|_{\mathbf{A}}$ has the following property: For any $\mathbf{x} \in K_s$,

$$\|\nabla \mathbf{x}\|_1 \leq \sqrt{s} \|\nabla \mathbf{x}\|_2 \leq \sqrt{8s} \|\mathbf{x}\|_2 \leq \sqrt{8s} \quad (29)$$

where the middle inequality applies $(x - y)^2 \leq 2x^2 + 2y^2$ and the fact that the maximal vertex degree in G is 4. Let $\mathbf{v}_1, \dots, \mathbf{v}_p$ be the bivariate Haar wavelet basis, and write the orthogonal decomposition $\mathbf{x} = \sum_k c_k \mathbf{v}_k$. Then, as $\|\mathbf{x}\|_2 \leq 1$, $\|\nabla \mathbf{x}\|_1 \leq \sqrt{8s}$, and $\sum_{k=1}^p 1/k \leq C \log p$, Lemma B.2 implies

$$\sum_{k=1}^p |c_k| \leq C \sqrt{s} \log p. \quad (30)$$

Each Haar vector \mathbf{v}_k is supported on a number $\alpha \in \{1, 2, 4\}$ of rectangular pieces of some size $|S| \times |T|$, with a constant value $\pm 1/\sqrt{\alpha|ST|}$ on each piece. Then Lemma B.1 implies for each (i, j)

$$|\mathcal{F}_{(i,j)}^* \mathbf{v}_k| \leq C \sqrt{\frac{1}{1 + \min(i-1, N_1 - i + 1)} \cdot \frac{1}{1 + \min(j-1, N_2 - j + 1)}}.$$

From the definition of ν and the bound $\sum_{k=1}^p 1/k \leq C \log p$,

$$\nu(j) \geq \frac{c}{(\log p)^2} \cdot \frac{1}{C_0 + \min(i-1, N_1 - i + 1)} \cdot \frac{1}{C_0 + \min(j-1, N_2 - j + 1)}$$

for a constant $c > 0$. Then from the definitions of \mathbf{A} and $\|\cdot\|_{\mathbf{A}}$, the bound (30), and the condition $1/K < N_1/N_2 < K$, we obtain

$$\|\mathbf{v}_k\|_{\mathbf{A}} \leq C(\log p)/\sqrt{n}, \quad \|\mathbf{x}\|_{\mathbf{A}} \leq B \equiv C(\log p)^2 \sqrt{s/n}. \quad (31)$$

As in [RV08, Theorem 3.3], we bound the covering number $N(K_s, \|\cdot\|_{\mathbf{A}}, v)$ in two ways: First, fix any $\mathbf{x} \in K_s$ and write now its Haar decomposition as

$$\mathbf{x} = \sum_{k=1}^p (a_k + \mathbf{i}b_k)\mathbf{v}_k$$

where $a_k, b_k \in \mathbb{R}$. Then for some universal constant $L > 0$, we obtain from (30)

$$\sum_{k=1}^p |a_k| + |b_k| \leq L\sqrt{s} \log p.$$

Applying Maurey's argument, define a discrete distribution over a random vector $\mathbf{z} \in \mathbb{C}^p$ by

$$\begin{aligned} \mathbb{P}\left[\mathbf{z} = L\sqrt{s} \log p \cdot \text{sign}(a_k)\mathbf{v}_k\right] &= \frac{|a_k|}{L\sqrt{s} \log p}, \\ \mathbb{P}\left[\mathbf{z} = L\sqrt{s} \log p \cdot \text{sign}(b_k)\mathbf{i}\mathbf{v}_k\right] &= \frac{|b_k|}{L\sqrt{s} \log p}, \\ \mathbb{P}\left[\mathbf{z} = 0\right] &= 1 - \sum_{k=1}^p \frac{|a_k| + |b_k|}{L\sqrt{s} \log p}. \end{aligned}$$

Then by construction, $\mathbb{E}[\mathbf{z}] = \mathbf{x}$. Letting $\mathbf{z}_1, \dots, \mathbf{z}_m$ be independent copies of \mathbf{z} , for a value m to be chosen later, Gaussian symmetrization yields (with all expectations conditional on \mathbf{A})

$$\mathbb{E} \left\| \mathbf{x} - \frac{1}{m} \sum_{j=1}^m \mathbf{z}_j \right\|_{\mathbf{A}} = \mathbb{E} \max_{r=1}^n \left| \frac{1}{m} \sum_{j=1}^m \mathbf{A}_r^* \mathbf{z}_j - \mathbb{E} \mathbf{A}_r^* \mathbf{z}_j \right| \leq \frac{C}{m} \mathbb{E} \max_{r=1}^n \left| \sum_{j=1}^m g_j \mathbf{A}_r^* \mathbf{z}_j \right| \quad (32)$$

for $g_1, \dots, g_m \stackrel{iid}{\sim} \mathcal{N}(0, 1)$. The bound (31) yields for every r

$$\sum_{j=1}^m |\mathbf{A}_r^* \mathbf{z}_j|^2 \leq \frac{Csm(\log p)^4}{n}.$$

Applying this to (32) with a Gaussian tail bound and union bound,

$$\mathbb{E} \left\| \mathbf{x} - \frac{1}{m} \sum_{j=1}^m \mathbf{z}_j \right\|_{\mathbf{A}} \leq C\sqrt{\log n} \cdot (\log p)^2 \sqrt{\frac{s}{mn}}.$$

For any $v > 0$, choosing $m = C(\log n)(\log p)^4 s / (nv^2)$ ensures this bound is at most v . Then by the probabilistic method, \mathbf{x} belongs to the $\|\cdot\|_{\mathbf{A}}$ -ball of radius v around some vector of the form $m^{-1} \sum_{j=1}^m \mathbf{z}_j$. The support of the distribution of \mathbf{z}_j has cardinality at most $2p+1$, and this support is the same for all $\mathbf{x} \in K_s$. Then there are at most $(2p+1)^m$ such vectors, so we obtain

$$\sqrt{\log N(K_s, \|\cdot\|_{\mathbf{A}}, v)} \leq \sqrt{m \log(2p+1)} \leq C\sqrt{s(\log n)(\log p)^5/n} \cdot 1/v. \quad (33)$$

We obtain a second covering bound by a union bound over \mathcal{S} : For any $\mathcal{S} = (S_1, \dots, S_k)$ with $|\partial\mathcal{S}| \leq s$, note that $k \leq s+1$. Define $\mathbf{U}_{\mathcal{S}} \in \mathbb{R}^{p \times k}$ such that its i th column is $\mathbf{e}_{S_i} / \sqrt{|S_i|}$ where $\mathbf{e}_{S_i} \in \{0, 1\}^p$ is the indicator of S_i . Then $\mathbf{U}_{\mathcal{S}}\mathbf{U}_{\mathcal{S}}^*$ is the projection onto $K_{\mathcal{S}}$, and

$$K_{\mathcal{S}} = \{\mathbf{U}_{\mathcal{S}}\mathbf{y} : \|\mathbf{y}\|_2 \leq 1\}.$$

As $\max\{\|\mathbf{U}_{\mathcal{S}}\mathbf{y}\|_{\mathbf{A}} : \mathbf{y} \in \mathbb{C}^k, \|\mathbf{y}\|_2 \leq 1\} \leq B$ by (31), a standard volume argument yields for $v \leq B$

$$N(K_{\mathcal{S}}, \|\cdot\|_{\mathbf{A}}, v) \leq (CB/v)^k.$$

The number of partitions \mathcal{S} with $|\partial\mathcal{S}| \leq s$ is at most $\sum_{j=0}^s \binom{[E]}{j} \leq (Cp)^{s+1}$. Applying $k \leq s+1$ and summing over \mathcal{S} ,

$$\sqrt{\log N(K_s, \|\cdot\|_{\mathbf{A}}, v)} \leq C\sqrt{s \log(CBp/v)}. \quad (34)$$

Returning to the entropy integral in (28), note that (31) implies $N(K_s, \|\cdot\|_{\mathbf{A}}, v) = 1$ for $v > B$, so the integral may be restricted to $v \in [0, B]$. Setting $t = 1/\sqrt{n}$, applying (34) for $v \in [0, t]$, and also applying Cauchy-Schwarz and $\log(B/t) \leq C \log p$, we get

$$\begin{aligned} \int_0^t \sqrt{\log N(K_s, \|\cdot\|_{\mathbf{A}}, v)} dv &\leq \sqrt{t} \cdot \sqrt{\int_0^t \log N(K_s, \|\cdot\|_{\mathbf{A}}, v) dv} \\ &\leq Ct \sqrt{s \left(1 + \log \frac{CBp}{t}\right)} \leq C \sqrt{\frac{s \log p}{n}}. \end{aligned}$$

Applying (33) for $v \in [t, B]$, we get

$$\int_t^B \sqrt{\log N(K_s, \|\cdot\|_{\mathbf{A}}, v)} dv \leq C \sqrt{s(\log n)(\log p)^7/n}.$$

Applying these bounds to (28) gives

$$E(\mathbf{A}) \leq C \sqrt{s(\log n)(\log p)^7/n} \cdot R(\mathbf{A}).$$

Taking now the expectation over \mathbf{A} and applying Cauchy-Schwarz and the triangle inequality,

$$\begin{aligned} \mathbb{E}[\kappa_s] &\leq \mathbb{E}[E(\mathbf{A})] \leq C \sqrt{s(\log n)(\log p)^7/n} \sqrt{\mathbb{E}[R(\mathbf{A})^2]} \\ &\leq C \sqrt{s(\log n)(\log p)^7/n} \sqrt{\mathbb{E}[\kappa_s] + 1}. \end{aligned}$$

This yields

$$\mathbb{E}[\kappa_s] \leq E(p, n, s) \equiv C \max \left(\sqrt{s(\log n)(\log p)^7/n}, s(\log n)(\log p)^7/n \right).$$

We now show concentration of each quantity κ_s around its mean. The argument is similar to [RV08, Theorem 3.9], and we omit some details. Write

$$\kappa_s = \left\| \sum_{r=1}^n \mathbf{A}_r \mathbf{A}_r^* - \mathbf{I} \right\|_{K_s}$$

where $\|\mathbf{M}\|_{K_s} = \sup_{\mathbf{x} \in K_s} |\mathbf{x}^* \mathbf{M} \mathbf{x}|$. Let \mathbf{A}' be an independent copy of \mathbf{A} and define

$$\gamma_s = \left\| \sum_{r=1}^n \mathbf{A}_r \mathbf{A}_r^* - (\mathbf{A}'_r)(\mathbf{A}'_r)^* \right\|_{K_s}.$$

Then by the same arguments as [RV08, Theorem 3.9], for any $t > 0$,

$$\mathbb{P}[\kappa_s \geq 2\mathbb{E}[\kappa_s] + t] \leq 2\mathbb{P}[\gamma_s \geq t], \quad \mathbb{E}[\gamma_s] \leq 2\mathbb{E}[\kappa_s] \leq 2E(p, n, s). \quad (35)$$

From (31), we have

$$\|\mathbf{A}_r \mathbf{A}_r^*\|_{K_s} \leq B^2$$

for every r . Then applying [RV08, Theorem 3.8], for any integers $l \geq q$, any $r > 0$, and some constants $C_1, C_2 > 0$,

$$\mathbb{P}[\gamma_s \geq 8q\mathbb{E}[\gamma_s] + 2B^2l + r] \leq (C_1/q)^l + 2 \exp \left(-\frac{r^2}{C_2 q \mathbb{E}[\gamma_s]^2} \right).$$

Let us assume without loss of generality $C_1 \geq 1/e$ and set $l = \lceil 2eC_1(\log n)(\log p)^3 \rceil$, $q = \lceil eC_1 \rceil$, and $r = 2\sqrt{C_2 q} \cdot 2E(p, n, s) \cdot t\sqrt{\log p}$, where $\lceil \cdot \rceil$ denotes the integer part. Then combining this with (35), we get for some constants $C, t_0 > 0$ and all $t > t_0$ that

$$\mathbb{P}[\kappa_s \geq C\sqrt{t} \cdot E(p, n, s)\sqrt{\log p}] \leq e^{-2(\log n)(\log p)^3} + 2e^{-4t(\log p)}.$$

Setting $\rho(s) = Cst(\log p)^8(\log n)/n$ for a sufficiently large constant $C > 0$, this yields

$$\mathbb{P}[\kappa_s \geq 2\sqrt{\rho(s)} + \rho(s)] \leq e^{-2(\log n)(\log p)^3} + 2e^{-4t(\log p)}.$$

The result follows from taking a union bound over $s = 1, \dots, |E|$, and noting $|E| \leq 2p$ and

$$2p \left(e^{-2(\log n)(\log p)^3} + 2e^{-4t(\log p)} \right) \leq e^{-(\log n)(\log p)^3} + p^{-t}$$

for all $t > t_0$ and sufficiently large $t_0 > 0$. □

APPENDIX C. RMSE FOR OPTIMAL PARAMETER TUNING

We report here the best-achieved RMSE, rather than RMSE for cross-validated selection of tuning parameters, corresponding to Tables 1, 2, 3, 4, and 5. For the 1-D signals, we performed 20 independent simulations, and we report also the standard deviations across these 20 simulations.

n/p		$\sigma = 0$	$\sigma = 1$	$\sigma = 2$	$\sigma = 3$	$\sigma = 4$	$\sigma = 5$	$\sigma = 6$	$\sigma = 7$
10%	ITALE	0.000	0.011	0.050	0.081	0.115	0.138	0.177	0.198
	TV	(0.000)	(0.004)	(0.024)	(0.023)	(0.033)	(0.034)	(0.031)	(0.025)
15%	ITALE	0.000	0.008	0.019	0.042	0.069	0.091	0.114	0.133
	TV	(0.000)	(0.002)	(0.007)	(0.016)	(0.023)	(0.029)	(0.028)	(0.029)
20%	ITALE	0.000	0.007	0.013	0.028	0.049	0.070	0.090	0.102
	TV	(0.000)	(0.002)	(0.003)	(0.012)	(0.019)	(0.019)	(0.017)	(0.020)
30%	ITALE	0.000	0.006	0.012	0.019	0.029	0.045	0.061	0.075
	TV	(0.000)	(0.001)	(0.003)	(0.006)	(0.009)	(0.014)	(0.011)	(0.013)
40%	ITALE	0.000	0.005	0.010	0.015	0.024	0.038	0.048	0.062
	TV	(0.000)	(0.001)	(0.002)	(0.003)	(0.007)	(0.012)	(0.015)	(0.016)
50%	ITALE	0.000	0.005	0.009	0.014	0.021	0.029	0.036	0.047
	TV	(0.000)	(0.001)	(0.002)	(0.003)	(0.006)	(0.011)	(0.013)	(0.013)

TABLE 6. Mean and standard deviation of best-achieved RMSE for the 1-D spike signal across 20 simulations

n/p		$\sigma = 0$	$\sigma = 1$	$\sigma = 2$	$\sigma = 3$	$\sigma = 4$	$\sigma = 5$	$\sigma = 6$	$\sigma = 7$
10%	ITALE	0.019 (0.081)	0.030 (0.066)	0.075 (0.055)	0.126 (0.057)	0.155 (0.064)	0.203 (0.059)	0.233 (0.070)	0.256 (0.068)
	TV	0.000 (0.000)	0.031 (0.005)	0.062 (0.011)	0.090 (0.016)	0.114 (0.018)	0.137 (0.021)	0.157 (0.022)	0.176 (0.024)
15%	ITALE	0.000 (0.000)	0.008 (0.002)	0.022 (0.011)	0.052 (0.023)	0.083 (0.027)	0.105 (0.030)	0.134 (0.027)	0.154 (0.035)
	TV	0.000 (0.000)	0.022 (0.003)	0.044 (0.006)	0.066 (0.009)	0.087 (0.011)	0.106 (0.013)	0.124 (0.014)	0.141 (0.016)
20%	ITALE	0.000 (0.000)	0.006 (0.001)	0.015 (0.006)	0.032 (0.011)	0.050 (0.016)	0.072 (0.023)	0.093 (0.027)	0.109 (0.027)
	TV	0.000 (0.000)	0.018 (0.002)	0.036 (0.004)	0.054 (0.007)	0.071 (0.009)	0.088 (0.011)	0.104 (0.012)	0.118 (0.013)
30%	ITALE	0.000 (0.000)	0.006 (0.001)	0.011 (0.002)	0.017 (0.004)	0.032 (0.010)	0.046 (0.012)	0.062 (0.015)	0.077 (0.015)
	TV	0.000 (0.000)	0.014 (0.001)	0.027 (0.003)	0.041 (0.004)	0.055 (0.005)	0.068 (0.007)	0.082 (0.008)	0.095 (0.010)
40%	ITALE	0.000 (0.000)	0.005 (0.001)	0.010 (0.002)	0.016 (0.004)	0.024 (0.009)	0.033 (0.012)	0.046 (0.014)	0.057 (0.017)
	TV	0.000 (0.000)	0.012 (0.001)	0.024 (0.002)	0.036 (0.003)	0.048 (0.005)	0.060 (0.006)	0.072 (0.007)	0.083 (0.008)
50%	ITALE	0.000 (0.000)	0.004 (0.001)	0.009 (0.002)	0.015 (0.005)	0.022 (0.009)	0.030 (0.011)	0.038 (0.012)	0.049 (0.018)
	TV	0.000 (0.000)	0.011 (0.001)	0.021 (0.003)	0.032 (0.004)	0.042 (0.005)	0.053 (0.007)	0.063 (0.008)	0.073 (0.009)

TABLE 7. Mean and standard deviation of best-achieved RMSE for the 1-D wave signal across 20 simulations

n/p		$\sigma = 0$	$\sigma = 4$	$\sigma = 8$	$\sigma = 12$	$\sigma = 16$	$\sigma = 20$	$\sigma = 24$	$\sigma = 28$
10%	ITALE	0.000	0.004	0.012	0.016	0.023	0.037	0.046	0.067
	TV	0.002	0.011	0.021	0.030	0.038	0.049	0.056	0.061
15%	ITALE	0.000	0.003	0.010	0.013	0.017	0.025	0.035	0.044
	TV	0.001	0.008	0.016	0.025	0.030	0.038	0.047	0.052
20%	ITALE	0.000	0.003	0.008	0.011	0.016	0.018	0.026	0.035
	TV	0.001	0.007	0.014	0.021	0.027	0.032	0.039	0.045
30%	ITALE	0.000	0.002	0.005	0.011	0.013	0.015	0.018	0.023
	TV	0.002	0.006	0.011	0.017	0.022	0.027	0.032	0.036
40%	ITALE	0.000	0.001	0.005	0.009	0.011	0.013	0.016	0.018
	TV	0.001	0.005	0.010	0.014	0.019	0.023	0.026	0.031
50%	ITALE	0.000	0.001	0.004	0.008	0.010	0.012	0.013	0.015
	TV	0.001	0.005	0.009	0.013	0.017	0.021	0.025	0.029

TABLE 8. Best-achieved RMSE for the Shepp-Logan phantom

n/p		$\sigma = 0$	$\sigma = 8$	$\sigma = 16$	$\sigma = 24$	$\sigma = 32$	$\sigma = 40$	$\sigma = 48$	$\sigma = 56$
10%	ITALE	0.000	0.002	0.010	0.028	0.042	0.058	0.077	0.093
	TV	0.002	0.014	0.028	0.041	0.054	0.064	0.077	0.085
15%	ITALE	0.000	0.001	0.007	0.017	0.030	0.043	0.057	0.075
	TV	0.001	0.011	0.022	0.032	0.043	0.053	0.063	0.071
20%	ITALE	0.000	0.001	0.005	0.012	0.025	0.034	0.047	0.054
	TV	0.001	0.009	0.019	0.028	0.037	0.044	0.055	0.061
30%	ITALE	0.000	0.001	0.002	0.007	0.014	0.024	0.033	0.043
	TV	0.001	0.007	0.016	0.022	0.030	0.038	0.044	0.052
40%	ITALE	0.000	0.000	0.002	0.005	0.010	0.018	0.026	0.032
	TV	0.001	0.007	0.013	0.019	0.026	0.032	0.039	0.043
50%	ITALE	0.000	0.001	0.002	0.004	0.007	0.012	0.019	0.027
	TV	0.001	0.006	0.011	0.017	0.023	0.029	0.034	0.040

TABLE 9. Best-achieved RMSE for the brain phantom

n/p		$\sigma = 0$	$\sigma = 4$	$\sigma = 8$	$\sigma = 12$	$\sigma = 16$	$\sigma = 20$	$\sigma = 24$	$\sigma = 28$
10%	ITALE	0.002	0.032	0.043	0.068	0.075	0.084	0.093	0.101
	TV	0.006	0.019	0.032	0.044	0.053	0.061	0.068	0.072
15%	ITALE	0.002	0.007	0.017	0.029	0.044	0.067	0.076	0.084
	TV	0.003	0.014	0.024	0.034	0.043	0.050	0.056	0.061
20%	ITALE	0.002	0.005	0.014	0.022	0.032	0.041	0.052	0.069
	TV	0.002	0.011	0.020	0.028	0.037	0.043	0.049	0.056
30%	ITALE	0.002	0.004	0.011	0.017	0.024	0.030	0.038	0.049
	TV	0.002	0.008	0.016	0.023	0.029	0.035	0.041	0.046
40%	ITALE	0.002	0.003	0.008	0.014	0.020	0.026	0.032	0.038
	TV	0.001	0.007	0.014	0.020	0.025	0.031	0.036	0.041
50%	ITALE	0.001	0.003	0.007	0.013	0.017	0.023	0.028	0.033
	TV	0.001	0.006	0.012	0.018	0.023	0.028	0.033	0.038

TABLE 10. Best-achieved RMSE for the XCAT chest slice phantom

REFERENCES

- [BD09] Thomas Blumensath and Mike E Davies. Iterative hard thresholding for compressed sensing. *Applied and Computational Harmonic Analysis*, 27(3):265–274, 2009.
- [BK04] Yuri Boykov and Vladimir Kolmogorov. An experimental comparison of min-cut/max-flow algorithms for energy minimization in vision. *IEEE Transactions on Pattern Analysis & Machine Intelligence*, 9:1124–1137, 2004.
- [BKM16] Dimitris Bertsimas, Angela King, and Rahul Mazumder. Best subset selection via a modern optimization lens. *The Annals of Statistics*, 44(2):813–852, 2016.
- [BRvdGZ13] Peter Bühlmann, Philipp Rütimann, Sara van de Geer, and Cun-Hui Zhang. Correlated variables in regression: clustering and sparse estimation. *Journal of Statistical Planning and Inference*, 143(11):1835–1858, 2013.
- [BT09] Amir Beck and Marc Teboulle. A fast iterative shrinkage-thresholding algorithm for linear inverse problems. *SIAM Journal on Imaging Sciences*, 2(1):183–202, 2009.
- [BVZ99] Yuri Boykov, Olga Veksler, and Ramin Zabih. Fast approximate energy minimization via graph cuts. In *Proceedings of the Seventh IEEE International Conference on Computer Vision*, volume 1, pages 377–384. IEEE, 1999.
- [CENR11] Emmanuel J Candès, Yonina C Eldar, Deanna Needell, and Paige Randall. Compressed sensing with coherent and redundant dictionaries. *Applied and Computational Harmonic Analysis*, 31(1):59–73, 2011.

- [CRT06a] Emmanuel J Candès, Justin Romberg, and Terence Tao. Robust uncertainty principles: Exact signal reconstruction from highly incomplete frequency information. *IEEE Transactions on Information Theory*, 52(2):489, 2006.
- [CRT06b] Emmanuel J Candès, Justin K Romberg, and Terence Tao. Stable signal recovery from incomplete and inaccurate measurements. *Communications on Pure and Applied Mathematics*, 59(8):1207–1223, 2006.
- [CX15] Jian-Feng Cai and Weiyu Xu. Guarantees of total variation minimization for signal recovery. *Information and Inference: A Journal of the IMA*, 4(4):328–353, 2015.
- [DHL17] Arnak S Dalalyan, Mohamed Hebiri, and Johannes Lederer. On the prediction performance of the Lasso. *Bernoulli*, 23(1):552–581, 2017.
- [Don06] David L Donoho. Compressed sensing. *IEEE Transactions on Information Theory*, 52(4):1289–1306, 2006.
- [EKDN18] Ethan R Elenberg, Rajiv Khanna, Alexandros G Dimakis, and Sahand Negahban. Restricted strong convexity implies weak submodularity. *The Annals of Statistics*, 46(6B):3539–3568, 2018.
- [EMR07] Michael Elad, Peyman Milanfar, and Ron Rubinstein. Analysis versus synthesis in signal priors. *Inverse Problems*, 23(3):947, 2007.
- [FG18] Zhou Fan and Leying Guan. Approximate ℓ_0 -penalized estimation of piecewise-constant signals on graphs. *The Annals of Statistics*, 46(6B):3217–3245, 2018.
- [FH94] Jeffrey A Fessler and Alfred O Hero. Space-alternating generalized EM algorithms for penalized maximum-likelihood image reconstruction. Technical report, Technical Report 286, Comm. and Sign. Proc. Lab., Dept. of EECS, Univ. of , 1994.
- [GHG⁺17] Changfei Gong, Ce Han, Guanghui Gan, Zhenxiang Deng, Yongqiang Zhou, Jinling Yi, Xiaomin Zheng, Congying Xie, and Xiance Jin. Low-dose dynamic myocardial perfusion CT image reconstruction using pre-contrast normal-dose CT scan induced structure tensor total variation regularization. *Physics in Medicine & Biology*, 62(7):2612, 2017.
- [HR16] Jan-Christian Hütter and Philippe Rigollet. Optimal rates for total variation denoising. In *Conference on Learning Theory*, pages 1115–1146, 2016.
- [KG19] Youngseok Kim and Chao Gao. Bayesian model selection with graph structured sparsity. *arXiv preprint arXiv:1902.03316*, 2019.
- [KKBG09] Seung-Jean Kim, Kwangmoo Koh, Stephen Boyd, and Dmitry Gorinevsky. ℓ_1 trend filtering. *SIAM review*, 51(2):339–360, 2009.
- [KT02] Jon Kleinberg and Eva Tardos. Approximation algorithms for classification problems with pairwise relationships: Metric labeling and markov random fields. *Journal of the ACM (JACM)*, 49(5):616–639, 2002.
- [KW14] Felix Krahmer and Rachel Ward. Stable and robust sampling strategies for compressive imaging. *IEEE Transactions on Image Processing*, 23(2):612–622, 2014.
- [LDP07] Michael Lustig, David Donoho, and John M Pauly. Sparse MRI: The application of compressed sensing for rapid MR imaging. *Magnetic Resonance in Medicine: An Official Journal of the International Society for Magnetic Resonance in Medicine*, 58(6):1182–1195, 2007.
- [LMRW18] Yuan Li, Benjamin Mark, Garvesh Raskutti, and Rebecca Willett. Graph-based regularization for regression problems with highly-correlated designs. In *2018 IEEE Global Conference on Signal and Information Processing (GlobalSIP)*, pages 740–742. IEEE, 2018.
- [NDEG13] Sangnam Nam, Mike E Davies, Michael Elad, and Rémi Gribonval. The cospase analysis model and algorithms. *Applied and Computational Harmonic Analysis*, 34(1):30–56, 2013.
- [NT09] Deanna Needell and Joel A Tropp. CoSaMP: Iterative signal recovery from incomplete and inaccurate samples. *Applied and Computational Harmonic Analysis*, 26(3):301–321, 2009.
- [NW13a] Deanna Needell and Rachel Ward. Near-optimal compressed sensing guarantees for total variation minimization. *IEEE Transactions on Image Processing*, 22(10):3941–3949, 2013.
- [NW13b] Deanna Needell and Rachel Ward. Stable image reconstruction using total variation minimization. *SIAM Journal on Imaging Sciences*, 6(2):1035–1058, 2013.
- [PB14] Neal Parikh and Stephen Boyd. Proximal algorithms. *Foundations and Trends® in Optimization*, 1(3):127–239, 2014.
- [Rin09] Alessandro Rinaldo. Properties and refinements of the fused lasso. *The Annals of Statistics*, 37(5B):2922–2952, 2009.
- [ROF92] Leonid I Rudin, Stanley Osher, and Emad Fatemi. Nonlinear total variation based noise removal algorithms. *Physica D: Nonlinear Phenomena*, 60(1-4):259–268, 1992.
- [RV08] Mark Rudelson and Roman Vershynin. On sparse reconstruction from Fourier and Gaussian measurements. *Communications on Pure and Applied Mathematics*, 61(8):1025–1045, 2008.
- [SSM⁺10] WP Segars, G Sturgeon, S Mendonca, Jason Grimes, and Benjamin MW Tsui. 4D XCAT phantom for multimodality imaging research. *Medical Physics*, 37(9):4902–4915, 2010.

- [TG07] Joel A Tropp and Anna C Gilbert. Signal recovery from random measurements via orthogonal matching pursuit. *IEEE Transactions on Information Theory*, 53(12):4655–4666, 2007.
- [Tib11] Ryan Joseph Tibshirani. *The solution path of the generalized lasso*. PhD thesis, Stanford University, 2011.
- [TSR⁺05] Robert Tibshirani, Michael Saunders, Saharon Rosset, Ji Zhu, and Keith Knight. Sparsity and smoothness via the fused lasso. *Journal of the Royal Statistical Society: Series B (Statistical Methodology)*, 67(1):91–108, 2005.
- [Ver10] Roman Vershynin. Introduction to the non-asymptotic analysis of random matrices. *arXiv preprint arXiv:1011.3027*, 2010.
- [WSST16] Yu-Xiang Wang, James Sharpnack, Alexander J Smola, and Ryan J Tibshirani. Trend filtering on graphs. *The Journal of Machine Learning Research*, 17(1):3651–3691, 2016.
- [XLXJ11] Li Xu, Cewu Lu, Yi Xu, and Jiaya Jia. Image smoothing via l_0 gradient minimization. *ACM Transactions on Graphics (TOG)*, 30(6):174, 2011.
- [Zha11] Tong Zhang. Sparse recovery with orthogonal matching pursuit under RIP. *IEEE Transactions on Information Theory*, 57(9):6215–6221, 2011.
- [ZWJ14] Yuchen Zhang, Martin J Wainwright, and Michael I Jordan. Lower bounds on the performance of polynomial-time algorithms for sparse linear regression. In *Conference on Learning Theory*, pages 921–948, 2014.